NOVA SCHOOL OF
SCIENCE & TECHNOLOGY

DEPARTMENT OF
PHYSICS

JOSÉ FRANCISCO GONÇALVES GRILO
BSc in Sciences of Physics Engineering

DETERMINATION OF THE EXCITATION FUNCTIONS FOR NUCLEAR REACTIONS INDUCED BY HELIUM-3 IN LITHIUM

MASTER IN PHYSICS ENGINEERING

NOVA University Lisbon
September, 2023

DEPARTMENT OF
PHYSICS

DETERMINATION OF THE EXCITATION FUNCTIONS FOR NUCLEAR REACTIONS INDUCED BY HELIUM-3 IN LITHIUM

JOSÉ FRANCISCO GONÇALVES GRILO
BSc in Sciences of Physics Engineering

Adviser: Prof Dr João Duarte Neves Cruz
Associate Professor, NOVA University Lisbon

Co-adviser: Dr Norberto José Sobral Catarino
Researcher, Instituto Superior Técnico, University of Lisbon

Examination Committee

Chair: Prof Dr Paulo António Martins Ferreira Ribeiro
Assistant Professor, NOVA University Lisbon

Rapporteur: Prof Dr Daniel Galaviz Redondo
Assistant Professor, Faculdade de Ciências, University of Lisbon

Adviser: Prof Dr João Duarte Neves Cruz
Associate Professor, NOVA University Lisbon

MASTER IN PHYSICS ENGINEERING

NOVA University Lisbon
September, 2023

Determination of the excitation functions for nuclear reactions induced by helium-3 in lithium

---

This document was created with the (pdf/Xe/Lua)LaTeX processor and the NOVAthesis template (v6.10.18) [1].

À minha família e amigos, que me relembraram
constantemente que tinha um trabalho para entregar.

ACKNOWLEDGEMENTS

I would like to thank Prof. João Cruz for all the support given throughout this work and for always being available to clarify any doubts or to share ideas. I also have to thank Dr. Norberto Catarino, Prof. Rui Coelho da Silva, Dr. Rodrigo Mateus and Dr. Eduardo Alves for the help and dedication shown to me.

I express my appreciation for Prof. Javier Ferrer for also being involved in the analysis of the ^{19}F(p,p)^{19}F cross section measurements.

A special thanks to Afonso Moutinho and Bruno Costa for letting me work, so many times, in the Instrumentation Laboratory of the Physics Department of the NOVA School of Science and Technology.

And last but not least, I really have to thank my family and my friends for constantly supporting me, in one way or another, in particular, to António Mendes, Diogo Durão, Eva Almeida and Gonçalo Baptista, who had a front row seat for this experience.

ABSTRACT

Since a few decades, nuclear fusion has been considered a promising alternative power source, but the technology behind it is still in a preliminary phase of development. Some technological challenges must still be overcome, namely in the components of the fusion reactor facing the plasma, where lithium might play an important role, especially as a tritium breeder, since tritium, an important isotope for nuclear fusion, is a scarce resource. Eventually, these components containing lithium will need to be characterized.

Therefore, in 2020, the International Atomic Energy Agency (IAEA) created a Coordinated Research Project (CRP) devoted to the "Development and Application of Ion Beam Techniques for Materials Irradiation and Characterization relevant to Fusion Technology" (CRP Code F11023).

The determination of the excitation functions for the nuclear reactions induced by ^{3}He in ^{6}Li, ^{7}Li, ^{9}Be, ^{10}B, ^{11}B, ^{12}C and ^{13}C was set as project priority due to lack of data and poor agreement among already existing datasets. The present work makes a contribution to the goals of the CRP by determining the excitation functions for the following nuclear reactions: ^{6}Li(^{3}He,p$_0$)^{8}Be, ^{7}Li(^{3}He,p$_i$)^{9}Be ($i = 0, 2, 3, 4$) and ^{7}Li(^{3}He,d$_0$)^{8}Be. The spectra were acquired using two thin lithium films (one of ^{6}Li and another of ^{7}Li) in the energy range between 800 keV and 2500 keV (the typical energy range for ion beam analysis techniques) for scattering angles between 115° and 165° with a 10° step. The results were compared with data from the literature.

Additionally, in this work, differential cross sections were determined for the elastic scattering of protons in ^{6}Li, ^{7}Li and ^{19}F in the energy range between 620 keV and 2050 keV and for a scattering angle of 165°.

Keywords: Cross section, Nuclear reactions, ^{3}He, ^{6}Li, ^{7}Li, Nuclear fusion, Material analysis

RESUMO

Desde há umas décadas atrás, a fusão nuclear tem sido considerada uma promissora fonte de energia alternativa, mas a tecnologia por detrás encontra-se ainda numa fase preliminar de desenvolvimento. Alguns obstáculos tecnológicos ainda têm de ser ultrapassados, nomeadamente os obstáculos associados às componentes do reator de fusão expostas ao plasma, onde o lítio poderá desempenhar um papel importante, especialmente como uma forma de produzir trítio, visto que o trítio, um isótopo importante para a fusão nuclear, é um recurso escasso. Eventualmente, estas componentes que contêm lítio terão de ser caracterizadas.

Por essa razão, em 2020, a Agência Internacional de Energia Atómica criou um programa coordenado de investigação dedicado ao desenvolvimento e aplicação de técnicas de feixes de iões para irradiação e caracterização de materiais revelantes para a tecnologia de fusão nuclear (*CRP Code F11023*).

A determinação das funções de excitação de reações nucleares induzidas por ^{3}He em ^{6}Li, ^{7}Li, ^{9}Be, ^{10}B, ^{11}B, ^{12}C and ^{13}C foi definida como uma das prioridades do projeto devido à falta de dados e à discrepância entre resultados de diferentes experiências. Este trabalho faz um contributo para atingir os objetivos do projeto ao se determinar as funções de excitação das seguintes reações nucleares: ^{6}Li(^{3}He,p$_0$)^{8}Be, ^{7}Li(^{3}He,p$_i$)^{9}Be ($i = 0, 2, 3, 4$) and ^{7}Li(^{3}He,d$_0$)^{8}Be. Os espetros foram adquiridos com dois filmes finos de lítio (um de ^{6}Li e outro de ^{7}Li) para um intervalo de energias entre 800 keV e 2500 keV (o intervalo de energias típico das técnicas analíticas de feixes de iões) para ângulos de dispersão entre 115° e 165° em incrementos de 10°. Posteriormente, os resultados foram comparados com resultados de experiências anteriores.

Adicionalmente, neste trabalho, secções eficazes diferenciais para a dispersão elástica de protões em ^{6}Li, ^{7}Li e ^{19}F foram determinadas no intervalo de energias entre 620 keV e 2050 keV e para um ângulo de dispersão de 165°.

Palavras-chave: Secção eficaz, Reações nucleares, ^{3}He, ^{6}Li, ^{7}Li, Fusão nuclear, Caracterização de materiais

CONTENTS

Appendices

List of Figures

List of Tables

1

Introduction

1.1 Motivation

The development of clean, efficient and safe technologies for energy production is essential to achieve a sustainable future for the planet, as an alternative to the ones dependant on fossil fuels and that, consequently, lead to the emission of greenhouse gases [2]. Since a few decades, nuclear fusion has been considered a promising alternative power source [3, 4]. In theory, nuclear fusion presents all the characteristics listed previously (clean, efficient and safe). However, in practice, the technology behind nuclear fusion is still in a preliminary phase of development. The International Thermonuclear Experimental Reactor (ITER) is intended to be the key experimental step between fusion research machines and future fusion power plants. It is planned that ITER's first operation takes place in December of 2025, but the reactor should only start fusing deuterium and tritium in 2035 [5]. The success of the ITER project and its operations will definitely determine the future of nuclear fusion as a viable energy source.

1.2 Relevance of Lithium for Fusion

Before ITER's operations start, some technological challenges must still be overcome. The components of the fusion reactor facing the plasma are going to be subjected to high thermal, mechanical and magnetic loads and, for that reason, the materials used for the structure of the tokamak must be carefully chosen. The development of nuclear fusion reactors is entering a phase in which Plasma Facing Components (PFCs) are the factor that will be responsible for limiting nuclear fusion's full potential. Nowadays, the PFCs used in tokamak reactors do not have the required radiation resistance properties needed to operate under the conditions of fusion reactors like the ITER.

To overcome this challenge, new PFC concepts have been proposed, in which the use of liquid lithium may play an important role by covering the PFCs [6, 7]. A good candidate solution for this problem is a Capillary-pore System (CPS) made of tungsten or molybdenum covered in liquid lithium [8].

The use of lithium (especially in liquid form) as PFC presents several advantages either in terms of preservation of the tokamak's structure, either in terms of plasma quality maintenance, such as:

- The low atomic number (Z) of lithium ensures that the quality of the plasma, which is mostly composed of hydrogen and helium, is not compromised.
- Lithium is in liquid state at the temperature of the walls of ITER while it is in operation (the melting point of lithium is 180.5 °C).
- The use of liquid lithium helps removing the heat at which the walls are subject to and allows for their self-regeneration, increasing the lifetime of the infrastructure.

1.2.1 Lithium as a Tritium Breeder

Besides the relevance of lithium as a crucial part of a PFC in future nuclear reactors, from a perspective of preservation of the infrastructure of the reactor, there is another reason why lithium is important in nuclear fusion.

In nuclear fusion (specifically, in a thermonuclear fusion reactor), the two main nuclear reactions are [9]:

$$\mathrm{D} + \mathrm{T} \longrightarrow {}^{4}\mathrm{He} + \mathrm{n} + 17.6\ \mathrm{MeV} \tag{1.1}$$

$$\mathrm{D} + \mathrm{D} \longrightarrow {}^{3}\mathrm{He} + \mathrm{n} + 3.27\ \mathrm{MeV} \tag{1.2}$$

From (1.1) and (1.2), it can be concluded that the deuterium-tritium (D-T) reaction generates about 5 times more energy than the deuterium-deuterium (D-D) reaction. In addition, the cross section for the D-T reaction is about 100 times greater than the one for the D-D reaction. These factors show that it is desirable that the D-T reaction occurs, but tritium is such a scarce resource in nature that the amounts available are not sufficient to fuel the reactor. In nature, tritium is formed by the interaction of cosmic rays with atmospheric gases and decays via a β^- process to ^{3}He ($t_{1/2}$ = 12.323 years) [9]. Tritium can (and is in many applications) be generated in fission nuclear reactions as a minor fission product (1 atom is generated in 10^4 fission processes).

So, in order to refuel the reactor, making it self-sufficient and, consequently, maintaining the stability of the operation, there is a need to develop the so called tritium breeding materials. Lithium is a key element in these materials, since it is possible to form tritium from lithium through the following nuclear reactions:

$$^{6}\mathrm{Li} + \mathrm{n} \longrightarrow \alpha + \mathrm{T} + 4.78\ \mathrm{MeV} \tag{1.3}$$

$$^{7}\mathrm{Li} + \mathrm{n} \longrightarrow \alpha + \mathrm{T} + \mathrm{n}' - 2.47\ \mathrm{MeV} \tag{1.4}$$

From (1.3) and (1.4) , it is concluded that the first reaction is exothermic and the second one is endothermic, whereby for low energy neutrons (thermal neutrons, for example) the first reaction might be preferred for tritium production. The previous statement is confirmed when both tritium production cross sections are compared. The cross section for reaction (1.3) is much greater than the one for the reaction (1.4), and it increases with decreasing neutron energy, with a maximum of 900 barn for thermal neutrons.

1.3 Relevance of ^{3}He Induced Nuclear Reactions

In section 1.2, it was mentioned that lithium might play a crucial role in future fusion power plants as a part of the PFC's.

Eventually, the PFC's will have to be characterized. The characterization of the PFC's will be performed by Ion Beam Analysis (IBA) Techniques, namely by ^{3}He-based nuclear reaction analysis (NRA). This technique consists of probing the sample with a beam of ^{3}He nuclei, which will induce nuclear reactions in the nuclei of the elements that constitute the sample. By detecting the particles emitted as a result of the nuclear reactions, it is possible to identify the elements that are present in the sample and their quantities.

There are other IBA techniques that could be used for this purpose, such as proton-based NRA or Rutherford Backscattering Spectroscopy (RBS). However, ^{3}He-based nuclear reaction analysis (NRA) has some advantages over these well-established techniques, in spite of ^{3}He being more expensive than ^{1}H and ^{4}He (RBS uses a ^{4}He beam to probe the sample). The problem with RBS is that it is not a sensitive technique to detect light elements (such as lithium) in a heavy matrix. In the case of proton-based NRA, it often leads to complex superimposed signals due to strong non-Rutherford cross sections for light elements [10, 11].

Due to the issues mentioned in the previous paragraph, it is important to study ^{3}He induced nuclear reactions in order to develop the ^{3}He-based NRA technique, so that materials relevant to fusion technology can be accurately characterized.

1.4 Objetives of the Present Work

In 2020, the International Atomic Energy Agency (IAEA) created a Coordinated Research Project (CRP) devoted to the "Development and Application of Ion Beam Techniques for Materials Irradiation and Characterization relevant to Fusion Technology" (CRP Code F11023) [12]. In this CRP, it was attributed high priority to the determination of the excitation function for nuclear reactions induced by ^{3}He in ^{6}Li, ^{7}Li, ^{9}Be, ^{10}B, ^{11}B, ^{12}C and ^{13}C.

The objective of the current work was to measure the differential cross sections for the nuclear reactions ^{6}Li(^{3}He,p$_0$)^{8}Be, ^{7}Li(^{3}He,p$_i$)^{9}Be ($i = 0, 1, 2, 3, 4$) and ^{7}Li(^{3}He,d$_0$)^{8}Be in the energy range between 800 and 2500 keV at six scattering angles: 115°, 125°, 135°, 145°, 155° and 165°. As can be seen in section 1.5, the current available data in the literature is very limited, whereby this work aims to make a contribution, either by validating (or not) previous results from the literature, either by producing new experimental data. The spectra aquisition took place in the RBS line of the 2.5 MV Van de Graaff accelerator at Centro Tecnológico e Nuclear (CTN) in Bobadela, Portugal.

The main goals of this work can be summarized as follows:

- Spectra aquisition on the Van de Graaff accelerator, with continuous beam and target stability monitoring.
- Development of a script in Python dedicated to spectra analysis, with features such as background estimation and removal (which is a key factor for an accurate determination of the excitation functions).
- Data analysis with the script referenced previously, with data from SRIM-2013 and with the software NDF [13, 14].
- Characterization of the targets using Rutherford Backscattering Spectrometry (RBS) and Time-of-Flight Elastic Recoil Detection Analysis (ToF-ERDA). Determination of the elemental depth profiles of the targets.
- Calculation of statistical and systematic uncertainties.
- Publish the obtained experimental results on a scientific journal in order to become available for the scientific community on the databases IBANDL and EXFOR [15].

1.5 State of the Art

Current data on cross sections available in the literature for the reactions $^{6}\text{Li}(^{3}\text{He}, \text{p}_i)^{8}\text{Be}$, $^{7}\text{Li}(^{3}\text{He}, \text{p}_i)^{9}\text{Be}$ and $^{7}\text{Li}(^{3}\text{He}, \text{d}_i)^{8}\text{Be}$ are not enough to extrapolate the cross sections to some angle and/or energy through simulation codes, such as SigmaCalc [16]. Table 1.1 contains the experiments that focused on measuring cross sections for these reactions [17–24]. Note that throughout this work, the energy or scattering/detection angle mentioned are the physical quantities relative to the laboratory reference frame, except at the end of section 2.1.2.1, where the energy in the center of mass frame is mentioned once.

From the experiments listed in table 1.1, some excitation functions were only determined for one detection angle and some only cover a limited energy range, neglecting certain energies of interest for IBA techniques.

The datasets from experiment [18] for the $^{6}\text{Li}(^{3}\text{He}, \text{p}_1)^{8}\text{Be}$ reaction contain only 4 points, which is not very useful, and the energy range is very limited. On the other hand, the experiments from [17, 20, 21, 23, 24] present results for many of the reactions of interest for this work for the appropriate energy range for IBA techniques and for a variety of scattering angles. All datasets are shown in Figure 4.10, alongside the results obtained in this work.

Table 1.1: Previous experiments in which the cross sections for the nuclear reactions induced by ^{3}He were determined

Author	Year	^{6}Li + ^{3}He Groups	^{7}Li + ^{3}He Groups	Energy Range (MeV)	Detection Angle	Number of Points
Schiffer *et al.* [17]	1956	p_0, p_1	-	0.89 - 5.08	150°	107, 99
Vignon *et al.* [18]	1969	p_0	-	0.76 - 1.91	150°	28
Vignon *et al.* [18]	1969	p_1	-	1.4 - 1.8	99.1°, 109°, 119.1°, 129.6°, 139.8°, 149.5°, 150°	6, 7
Lru [19]	1972	-	p_0, p_1, p_2, p_4	1.79 - 2.99	120°	13
Bondouk *et al.* [20]	1975	-	p_0, p_2	0.99 - 2.44	130°	70, 72
Bondoul *et al.* [21]	1977	-	d_0	1 - 2.54	130°	74
Elwyn *et al.* [22]	1980	p_0	-	0.46 - 1.85	90°, 100°, 105°, 110°, 120°, 134.9°, 145°, 155°	17, 13, 2, 13, 16, 17, 14
Rath *et al.* [23]	1990	-	p_0	1 - 2.5	120°, 140°, 160°	4
Rath *et al.* [23]	1990	-	p_2	0.6 - 2.48	360°	4
Zhu *et al.* [24]	2021	p_0	p_0, p_1, p_2, $p_{3,4}$, d_0	1.18 - 2.98	146°	19, 18

1.6 (p,p) Reactions in ^{6}Li, ^{7}Li, ^{19}F

Despite the main topic of this dissertation being the determination of the excitation functions of nuclear reactions induced by ^{3}He in lithium, a contribution to another project was made during the same time. This section aims to explain this project and its motivation.

Ion beam analysis (IBA) methods strongly rely on the available cross section data. Consequently, precise determation of the excitation functions is required in order to obtain reliable results with IBA techniques.

A large number of excitation functions for nuclear reactions have been measured and can be found in IBANDL database [15]. However, for some nuclear reactions, reported cross section values present numerous discrepancies. One of these reactions is the proton elastic scattering in fluorine, which was pointed out by A. F. Gurbich in 2010 [25], reason why there is a need for new measurements. The existing experimental data from different authors for this reaction at scattering angles between 159° and 165° are in poor agreement. The theoretical curves for these scattering angles are identical, so the difference between the data from different authors cannot be explained by the experimental data from cross section angular dependence. Figure 1.1 contains an evaluation performed by Gurbich at $\theta = 162°$ (solid line) and experimental data points from different authors [26–30] for the ^{19}F(p,p)^{19}F reaction.

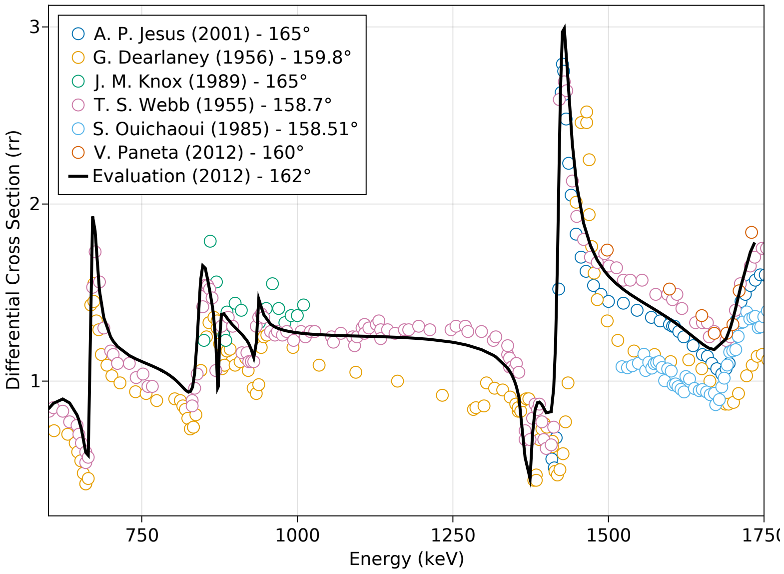

Figure 1.1: Comparison of the evaluated cross section for the ^{19}F(p,p)^{19}F reaction (solid line) with experimental data (dots)

That said, the objective of this project was to make new measurements of differential cross sections for the ^{19}F(p,p)^{19}F reaction in the energy range between 620 and 2050 keV at 165°. The data aquisition also took place in the RBS line of the 2.5 MV Van de Graaff accelerator at CTN.

Since a thin LiF (lithium fluoride) film evaporated on top of a silver thin layer was used for the measurements, the excitation functions for the nuclear reactions ^{6}Li(p,p)^{6}Li and ^{7}Li(p,p)^{7}Li were also determined and compared with previous experimental data from other authors [31–33].

The goals for this project were practically identical to the ones from the main topic of this dissertation, except that, for data analysis, the software used was SIMNRA [34] instead of NDF and that the target was characterized with RBS data exclusively.

2

THEORETICAL BACKGROUND OF THE EXPERIMENT

2.1 Nuclear Physics Overview

2.1.1 Basic Concepts

In the laboratory, a nuclear reaction happens when an incident particle a (commonly called projectile) collides with a nucleus X (usually, stationary) from a sample (the target). There is a probability that an emitted particle b (the particle that is detected in an experiment) and a residual nucleus Y may result from the collision of particles a and X. Expressions (2.1) and (2.2) are two different ways of representing a nuclear reaction, where the second one is a more compact notation:

$$a + X \longrightarrow b + Y \tag{2.1}$$

$$X(a, b)Y \tag{2.2}$$

The Q-value of a reaction, i.e. the energy released in a reaction is given by:

$$Q = T_Y + T_b - T_a - T_X = (m_a + m_X - m_Y - m_b)c^2 \tag{2.3}$$

where T_i is the kinetic energy of particle i, m_i is the mass of the particle and c is the speed of light in vacuum ($c^2 = 931.494$ MeV/u - u stands for unified atomic mass unit and is defined as $\frac{1}{12}$ of the mass of an unbound neutral atom of ^{12}C). Equation (2.3) comes simply from the conservation of energy and from Einstein's equivalence between mass and energy.

If the residual nucleus Y is not in the ground state, the Q-value can be calculated as follows:

$$Q = Q_0 - E_{ex} \tag{2.4}$$

where Q_0 is the Q-value of the reaction when Y is in the ground state and E_{ex} is the excitation energy of the excited state the residual nucleus is on.

To identify the peaks in a spectrum, it is often necessary to calculate the kinematics of a reaction. As said before, particle b is the one that reaches the detector, hence the kinetic energy that needs to be known is the one from particle b. By applying the laws of conservation of energy and momentum to the reaction, it is possible to get equation (2.5), which allows for the determination of the kinetic energy of particle b for a detection angle θ (assuming that $T_x = 0$):

$$\sqrt{T_b} = \frac{\sqrt{m_a m_b T_a} \cos\theta \pm \sqrt{m_a m_b T_a \cos^2\theta + (m_b + m_Y)[m_Y Q + (m_Y - m_a)T_a]}}{m_Y + m_b} \tag{2.5}$$

2.1.2 Cross Sections

The most important concept to understand for this work is the concept of cross section, and the concept of differential cross section in particular. The cross section is a measure of the probability that a specific phenomenon (for example, a nuclear reaction) will take place under certain experimental conditions (energy of the particles of the beam and/or detection angle, for example).

In an experiment, for a beam of I_a particles per unit time whose particles collide with a target that has an areal density N (in particles of X per unit area) and where the detection of b particles happens at a rate of detection R_b, the cross section (which has units of area) can be calculated as:

$$\sigma = \frac{R_b}{I_a N} \tag{2.6}$$

Since detectors only occupy a small solid angle $d\Omega$, it is necessary to take it into account. That is where the concept of differential cross section comes in handy. In this case, by following an analogous reasoning it is possible to get to the expression:

$$\frac{d\sigma}{d\Omega} = \frac{Ye}{N\Omega Q} \tag{2.7}$$

where Y is the yield of the reaction (that is the number of events detected), e is the elementary charge, N is the areal density of the element in the target, Ω is the solid angle of the detector (in units of sr) and Q is the accumulated charge (in units of C). Note that the differential cross section is in units of area per steradian (usually, mb/sr).

Equation (2.7) is the basis for any excitation function determination experiment for Nuclear Reaction Analysis (NRA) or Elastic Backscattering Spectrometry (EBS), as long as the sample is a thin target. In fact, this is the equation used for the calculation of the cross sections in the ^{3}He induced reactions experiment.

To apply equation (2.7), it is necessary to determine the accumulated charge Q for every single run. In the ^{3}He induced reactions experiment, this was made by using the software NDF to fit the RBS spectra that were being acquired simultaneously with the NRA spectra (read section 3.1.1 for a detailed explanation of the aquisition system).

However, it is possible to calculate the differential cross section without needing to determine the accumulated charge Q by comparing the yield of the peak of interest with another peak of the spectrum corresponding to a reaction whose excitation function is well established. In the proton elastic scattering experiment, the peak used for normalization was the one corresponding to the reaction Ag(p,p)Ag (read chapter 4 for a detailed description of the target and the spectra acquired), since, for the energy range used, the interaction between a proton and a Ag nucleus is purely coulombian due to the high Z of Ag, i.e. the excitation function of this reaction is described by the Rutherford cross section formula (equation (2.10)).

As mentioned before, the alternative method of calculating the differential cross sections was applied in the proton elastic scattering experiment. Since the peak corresponding to the reaction Ag(p,p)Ag was used for normalization, the first step was to determine the stoichiometric factor n, which consists of the ratio between the amount of the element being studied (for example, ^{19}F in the case of the reaction ^{19}F(p,p)^{19}F) and the amount of the normalizing element (in this case, Ag). For this purpose, a RBS spectrum (acquired with a ^{4}He^{+} beam) was analysed because it allows for a precise determination of the amounts of the elements due to the fact that differential cross sections follow equation (2.10). The stoichiometric factor n is calculated as follows from equation (2.7):

$$n = \frac{N_{\mathrm{F}}}{N_{\mathrm{Ag}}} = \frac{\frac{Y_{\mathrm{F}} e}{\sigma_{R_{\mathrm{F}}}(\theta)\Omega Q}}{\frac{Y_{\mathrm{Ag}} e}{\sigma_{R_{\mathrm{Ag}}}(\theta)\Omega Q}} = \frac{Y_{\mathrm{F}}}{Y_{\mathrm{Ag}}} \frac{\sigma_{R_{\mathrm{Ag}}}(\theta)}{\sigma_{R_{\mathrm{F}}}(\theta)} \tag{2.8}$$

After calculating the stoichiometric factor n, it is now possible to calculate the differential cross section of the reaction with a reasoning similar to the one followed in equation (2.8).

$$n = \frac{Y_{\mathrm{F}}}{Y_{\mathrm{Ag}}} \frac{\sigma_{R_{\mathrm{Ag}}}(\theta)}{\sigma_{\mathrm{F}}(\theta)} \Leftrightarrow \sigma_{\mathrm{F}}(\theta) = \frac{Y_{\mathrm{F}} \times \sigma_{R_{\mathrm{Ag}}}(\theta)}{Y_{\mathrm{Ag}} \times n} \tag{2.9}$$

Note that in equation (2.9), the cross section for the reaction Ag(p,p)Ag is given by the Rutherford cross section formula (equation (2.10)). Even when considering equation (2.9) generically, the differential cross section that appears in the numerator usually is of a reaction which follows the Rutherford cross section formula, because it is necessary that the cross section in the numerator is well known so that equation (2.9) is valid. From equation (2.9), the cross sections are obtained in units of mb/sr. To calculate these same cross sections in rr (ratio-to-Rutherford), we simply divide equation (2.9) by the Rutherford cross section of the reaction being studied (the Rutherford cross section does not correspond to the real cross section, but the point of dividing by it is to compare the real value of the cross section with the value of the Rutherford cross section, which would correspond to the real value if the interaction between the particles in the reaction was purely coulombian).

2.1.2.1 Rutherford Scattering Differential Cross Section Formula

Rutherford scattering is the elastic scattering of charged particles by the Coulomb interaction, i.e. it is a phenomenon where particles are scattered exclusively due to electromagnetic interaction, without the influence of the nuclear potential.

This is a well understood phenomenon, which can be explained/studied classically or quantum mechanically. An important parameter that can be calculated in one way or another (and that gives the exact same result in both) is its differential cross section, given by equation (2.10).

$$\sigma_R(\theta) = \left(\frac{Z_1 Z_2 e^2}{4E}\right)^2 \frac{4}{\sin^4\theta} \frac{(\cos\theta + \sqrt{1-(M_1/M_2)^2\sin^2\theta})^2}{\sqrt{1-(M_1/M_2)^2\sin^2\theta}} \quad [\mathrm{cm}^2/\mathrm{sr}] \tag{2.10}$$

where Z_1 and Z_2 are the atomic numbers of the projectile and the target, respectively, e is the elementary charge ($e^2 = 1.44 \times 10^{-13}$ MeV $\cdot$ cm), θ is the detection angle and M_1 and M_2 are the atomic masses of the projectile and the target, respectively.

Despite equation (2.10) allowing to calculate the differential cross section for Rutherford scattering, it does not take into account the electron screening effect. Among the analytical screening models that correct the Rutherford cross section, the one that was used in the present work was L'Ecuyer correction term [35], given by equation (2.11).

$$\sigma_{R_{cor}}(\theta) = \left(1 - \frac{0.049 Z_1 Z_2^{4/3}}{E_{\mathrm{CM}}}\right)\sigma_R(\theta) \tag{2.11}$$

where E_{CM} is the energy of the incident particle in the center of mass frame.

A more in-depth explanation of these concepts can be found in [36].

3

MATERIALS AND METHODS

3.1 Experimental Procedure

As stated in section 1.4, the measurements of both experiments (the ^{3}He induced nuclear reactions and the proton elastic scattering experiment) were conducted in the RBS line of the 2.5 MV Van de Graaff particle accelerator that is located at CTN. While the measurements for the ^{3}He induced reactions were performed in the universal chamber, the ones performed for the proton elastic scattering experiment ocurred in the small chamber. Figure 3.1 illustrates the Van de Graaff accelerator that is located at Campus Tecnológico e Nuclear (CTN), Bobadela, Portugal.

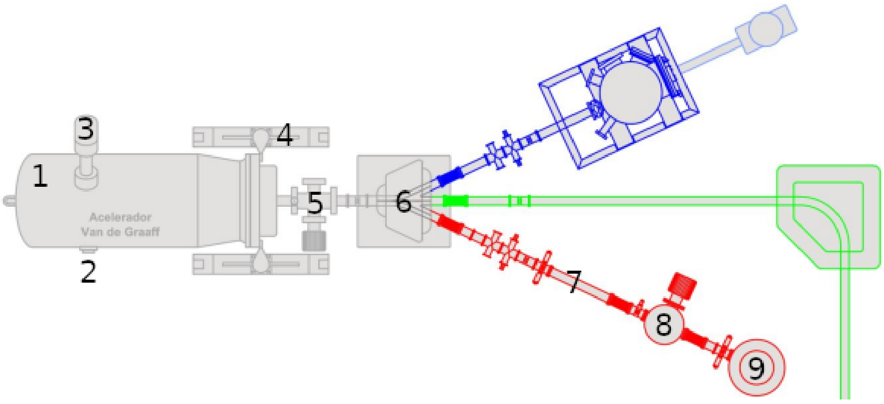

Figure 3.1: Layout of the Van de Graaff accelerator at CTN. The RBS line is represented in red. (1 - Pressure Vessel; 2 - Voltmeter; 3 - Corona; 4 - Supporting Structure; 5 -Transport System; 6 - Magnetic Analyser; 7 - RBS Line; 8 - Small Chamber; 9 - Universal Chamber) Original figure from [37]

3.1.1 ^{3}He Induced Nuclear Reactions

For the ^{3}He induced reactions experiment, the energy scan was performed in steps of 100 keV for beam energies between 800 and 2500 keV, in which 80 energy points were acquired (but since that for every run, three detectors at different angles were acquiring data, the total number of spectra produced was 240). The NRA detectors were placed at angles of 115°, 135° and 155° in one configuration and of 125°, 145° and 165° in another. In front of each detector, a 12 μm foil of mylar was placed in order to stop the elastically scattered ^{3}He particles from reaching the detectors, because, since the cross section for elastic scattering is greater than the cross sections measured in the experiment, there would be a significant increase in the dead time of the NRA detectors. An additional fixed RBS detector was placed in order to determine the accumulated charge, Q, for each run. Figure 3.2 shows the experimental setup at the universal chamber.

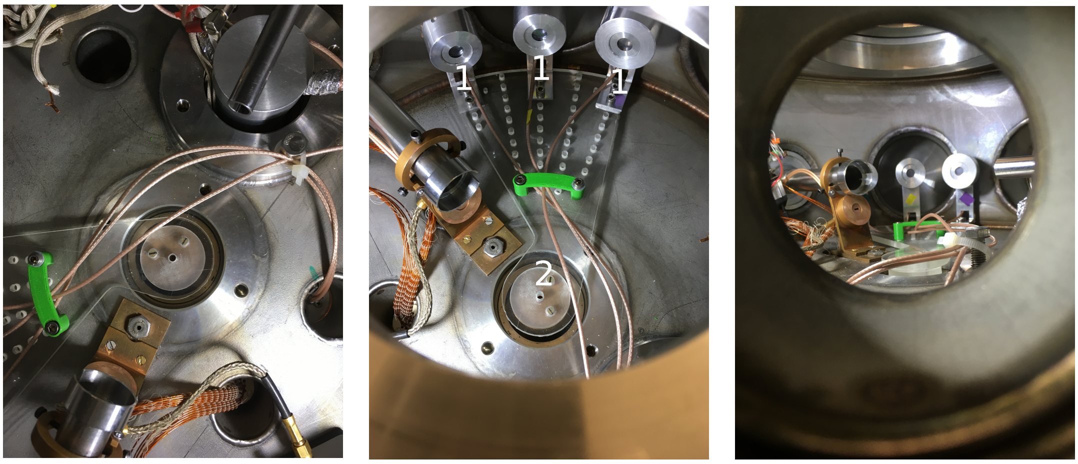

(a) Top View (b) NRA Detectors (c) Lateral View

Figure 3.2: Photographs of the Universal Chamber (1 - Particle Detectors; 2 - Rotatable Plate)

In this experiment, two different implanted targets were produced in the implanter at CTN: one target of ^{6}Li and other of ^{7}Li, both implanted into aluminium (this last target was previously used in ^{7}Li reaction measurements by J. Cruz [32]).

3.1.2 Proton Elastic Scattering Reactions

For the proton elastic scattering experiment, the energy scan was performed in steps of ≈ 10 keV, except near resonance zones where the steps were from $2-4$ keV. A total of 204 runs were performed, for beam energies between 620 and 2050 keV. In the small chamber, three detectors were placed. One detector was placed at a scattering angle of 140° and the other two at 165°, one in each side of the chamber. However, due to poor resolution of two of the detectors (the 145°-detector and one of the detectors at 165°), only the data from one detector was analyzed.

For this experiment, it was necessary to produce the self-supported thin targets where the nuclear reactions took place. For this purpose, the thermal evaporator at CTN, which can be seen in Figure 3.3, was used to, firstly, evaporate the silver thin films (this silver layer serves as a support for the other layer). Then, 99% pure LiF (lithium fluoride) was evaporated on top of the silver thin films. These evaporations were performed under a vacuum of approximately 10^{-6} mbar in order to minimize contamination by other elements, namely carbon and oxygen. The vacuum system is composed by a rotary pump and a diffusion pump.

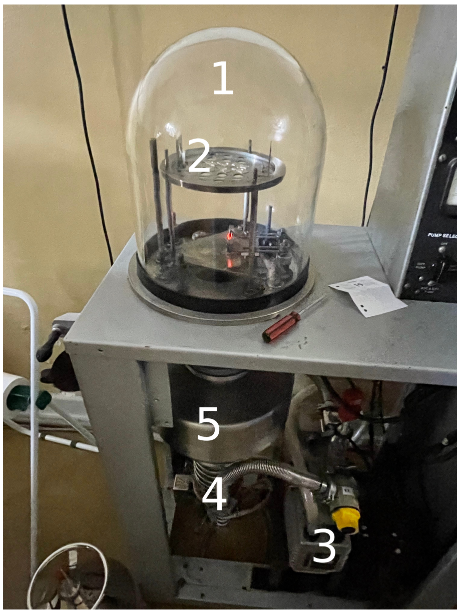

Figure 3.3: Thermal Evaporator at CTN (1 - Vacuum Bell Jar; 2 - Support with the Targets; 3 - Rotary Pump; 4 - Diffusion Pump; 5 - Liquid Nitrogen Trap)

3.2 Background Estimation and Removal

In section 1.4, it was mentioned that background determination and removal is a key factor for accurate cross sections determination and has been a major issue in spectroscopy for years. Nowadays, the high demand for even more precise experimental results and accurate uncertainty calculations is responsible for an increased concern in solving this problem.

In the present work, the source of background in the spectra acquired is a phenomenon called plural scattering, which consists on the large angle scatterings of the particles emitted in nuclear reactions that happen inside the material before reaching the detector, resulting in the low-energy tails of some peaks in a spectrum [38].

3.2.1 SNIP Algorithm

Different solutions for this problem have been proposed. One of the most promising methods is the Statistics-sensitive Non-linear Iterative Peak-clipping (SNIP) algorithm. It has even been considered the most efficient method for background removal [39].

The SNIP algorithm was first proposed by Ryan, in 1988 [40]. With SNIP, the background is calculated iteratively in order to obtain $v_1(i)$, $v_2(i)$, up to $v_m(i)$, where $v_j(i)$ is the value of the background in channel i and iteration j and m is a parameter given by the user and that should translate the relation

$$2m + 1 = w \tag{3.1}$$

where w corresponds to the full width at half maximum (FWHM) of a peak. To calculate the value of background in channel i in the p-th iteration, the following equation is used:

$$v_p(i) = \min\left\{v_{p-1}(i), \frac{1}{2}[v_{p-1}(i+p) + v_{p-1}(i-p)]\right\} \tag{3.2}$$

Still in 1988, it was proposed the application of the LLS operator (LLS stands for "Logarithm Logarithm Square-root") to the raw spectrum data before executing the SNIP algorithm in order to enhance small peaks by reducing differences between peaks with different orders of magnitude. The LLS operator is given by:

$$v(i) = \log\left(\log\left[\sqrt{y(i)+1}+1\right]+1\right) \tag{3.3}$$

where $y(i)$ is the number of counts in channel i. After estimating the background, it is necessary to apply the inverse LLS operator in order to obtain the resulting baseline of the original spectrum [40].

In the years that followed, Morháč developed the algorithm further by generalizing it to multidimensional spectra, adding an incorporated smoothing method to the algorithm, and incorporating other features [41, 42].

Figure 3.4 shows an example of a background estimated by the SNIP algorithm with $m = 10$. The y-axis of the figure is shown in logarithmic scale.

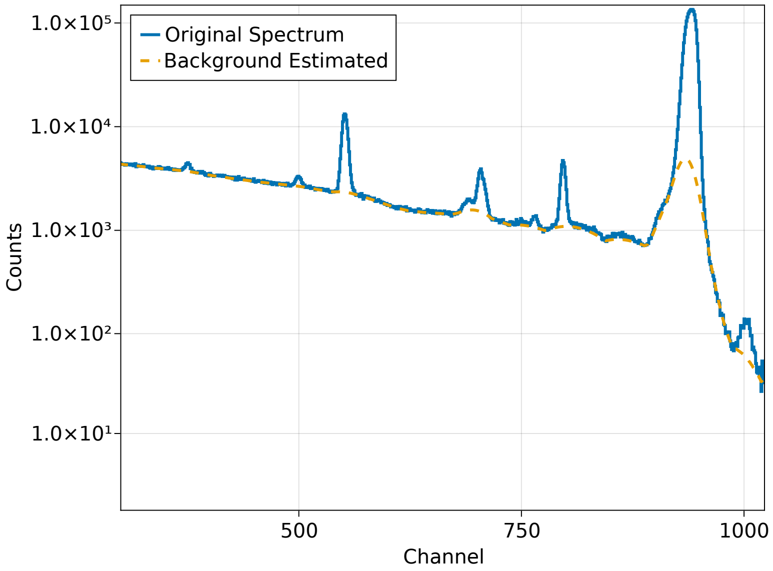

Figure 3.4: SNIP background estimation for $m = 10$

From Figure 3.4, it becomes evident the effect that parameter m has on the background estimation, by comparing the background estimated below peaks with different widths.

3.2.2 SASNIP Algorithm

In 2018, Shi *et al.* [43] proposed a variant of the algorithm in which the user no longer introduces parameter m, which is the main source of error in conventional SNIP. Instead, the algorithm uses a first derivative peak search algorithm to determine the peak region of each peak present in the spectrum. The vector containing the information of the peak regions should look like:

$$r = [0, ..., 0, w_1, ..., w_1, 0, ..., 0, w_2, ..., w_2, ..., 0, ..., 0, w_k, ..., w_k, 0, ..., 0] \tag{3.4}$$

where w_k represents the width of the k-th peak region and r has the same length as the spectrum. Then, parameter m is defined from vector r by:

$$m = \max\{w_j\}, j \in [1, k] \tag{3.5}$$

With parameter m determined, an adaptive-to-peak-region-width SNIP algorithm is defined:

$$v_p(i) = \begin{cases} \min\left\{v_{p-1}(i), \frac{1}{2}[v_{p-1}(i+p) + v_{p-1}(i-p)]\right\}, \text{if } p \leq r(i) \\ v_{p-1}(i), \text{if } p > r(i) \end{cases} \tag{3.6}$$

After executing the adaptive-to-peak-region-width SNIP algorithm, the following parameters are calculated:

$$B_{n+1} = \omega \sum v_{in}(i) + (1 - \omega) \sum v_{out}(i) \tag{3.7}$$

$$\omega = \frac{\sum v(i)}{\sum y(i)} \tag{3.8}$$

where $v_{in}(i)$ is the value of the background of channels where $r_i \neq 0$, $v_{out}(i)$ is the value of the background of channels where $r_i = 0$, and y(i) is the value of the original spectrum in channel i. From B_{n+1}, a comparison with the previous estimated background is made by calculating:

$$\frac{|B_n - B_{n+1}|}{B_n} \tag{3.9}$$

If the value of expression (3.9) is less or equal to a tolerance given by the user (0.5%, for example), the algorithm stops since the desired background was already estimated, otherwise the adaptive-to-peak-region-width SNIP algorithm is applied to the last background estimated.

This last step concludes the variant of SNIP introduced by Shi, called Step-Approximation Statistics-sensitive Non-linear Iterative Peak-clipping (SASNIP). The advantage of using this variant of SNIP is that parameter m is determined by the peak search algorithm, reducing greatly the error in the background estimation, since it no longer depends on the user. The only parameter that the user inserts in the algorithm is the tolerance, despite the use of 0.5% being recommended.

3.2.2.1 Comments on the SASNIP algorithm

While it was not necessary to the implement the SNIP algorithm (because it is implemented in a Python library called pybaselines [44]), the SASNIP algorithm had to be implemented from scratch, so the comments made in this section are more related to the implementation, which is not perfect, than to the algorithm itself.

The algorithm strongly relies on the first derivative peak search algorithm, which in turn relies on numerical differentiation, which has its limitations. It was found that the implemented first derivative peak search algorithm was not always able to determine the boundaries of the peaks correctly, this when the algorithm identified the existence of a peak at all.

Additionally, it was necessary to add a threshold value that the derivative of the spectrum needed to cross in order to separate noise from actual peaks.

The algorithm worked fairly well in the proton elastic scattering spectra, but it was not possible to apply it to the ^{3}He-induced nuclear reactions spectra, in which the SNIP algorithm ended up being used.

In conclusion, the SASNIP algorithm may be a good replacement for the SNIP algorithm, because it solves the free parameter m problem. However, further development has to be made in order to make it generally viable, namely in the algorithm responsible for identifying the peak regions.

The SASNIP algorithm implemented in this work, as well as the software used for analyzing the spectra can be found at a GitHub repository.

Note: the code written is not optimized, well organized or well commented, but it was useful for the current work. Hopefully, in the future, a better version of the software will get released.

3.2.3 Background Fitting

For the majority of cases, the algorithms described in the previous sections were the prefered methods of background estimation. However, for a case in particular, fitting a function to the background locally was a method that provided better results.

In the proton elastic scattering experiment, for low beam energies, the ^{19}F peak starts overlapping with the Ag peak (see Section 4.2.2, which helps interpret the spectra). For these cases, the (SA)SNIP algorithm becomes inefficient at removing the background.

To solve this problem, the silver background was fitted by a sum of two exponentials and a Voigt function (equation (3.10)) [32].

$$f(x) = A_1 \exp^{-x/\tau_1} + A_2 \exp^{-x/\tau_2} + \frac{A_3 Re[w(z)]}{\sigma\sqrt{2\pi}} \tag{3.10}$$

$$z = \frac{x - \mu + i\gamma}{\sigma\sqrt{2}} \tag{3.11}$$

$$w(z) = \exp^{-z^2} \operatorname{erfc}(-iz) \tag{3.12}$$

where A_1, A_2, A_3, τ_1, τ_2, μ and σ are free parameters.

The fit was performed locally in the 8 spectra with the lowest beam energies. Figure 3.5 shows one of the spectra in which the fit was performed, where it is possible to compare the background estimated with the fitting method with the one estimated with the SNIP algorithm. It is possible to conclude that a better background estimation can be achieved by fitting the background.

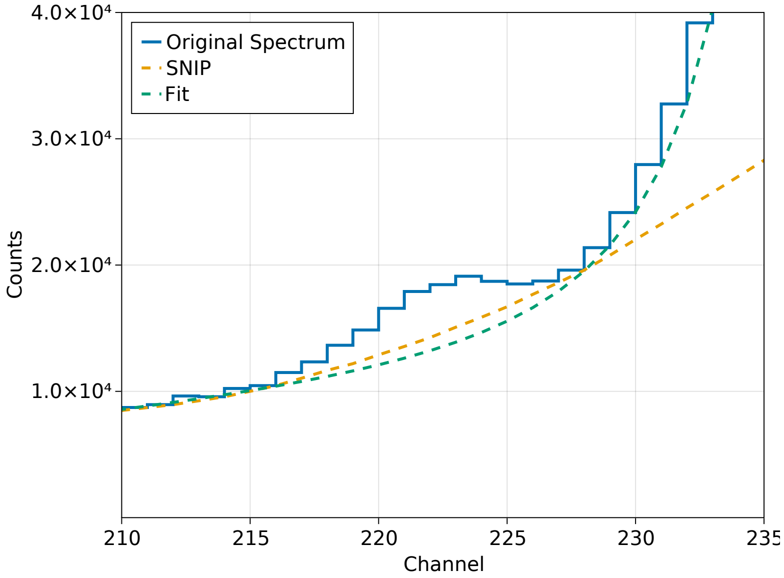

Figure 3.5: Comparison between the SNIP algorithm and the fit made to the background

The major drawback of this method is that it is more time consuming, due to the fact that it is more difficult to get the ideal fit than it is to use the (SA)SNIP algorithm (which, in the worst case, consists of changing the free parameter m).

4

DATA ANALYSIS AND RESULTS

This chapter will focus on the data analysis methods used in both projects, in the calculation of uncertainties and in the discussion of results.

Since both projects are similar in nature, the steps followed were pratically the same, although the methods used to complete these steps may differ. Therefore, some sections will be divided by project in order to clarify which method was used in which project. One example of this is section 4.3, where the methods used to calculate the effective energy of each run for each project are explained.

4.1 Target Composition Determination

To know the composition of a target is really important in an experiment where the main goal is the accurate determination of excitation functions.

If equation (2.7) is used directly to calculate differential cross sections, the importance of determining the amount of the element that takes part in the nuclear reaction (in this case, lithium) present in the sample becomes evident (if, otherwise, equation (2.9) is used, maybe it is not directly evident, but to use it, it is necessary to calculate the stoichiometric factor n - by applying equation (2.8) - which is a ratio of areal densities of two elements present in a sample).

In the previous paragraph, it was discussed the importance of simply determining the amount of the elements present in the sample. However, it is also important to determine the depth distribution of these elements. The whole purpose - or part of it, at least - of using IBA techniques is to characterize a material, i.e. to extract as much information about a material as possible, which includes knowing which elements are present, in which amounts and where in the sample. However, in this work, the main goal is to determine excitation functions, as stated before. Nevertheless, the determination of the depth profile of the targets contributes to the execution of intermediate steps that lead to the end goal. For example, determining the depth profiles of the targets accurately:

- is mandatory in order to determine the effective charge in a run;

- helps interpreting spectra and identifying the peaks that are part of them (see section 4.2).

The approaches followed to determine the composition of the targets, which were different in both projects, will be explained in the next subsections.

4.1.1 ^{3}He Induced Nuclear Reactions

In the ^{3}He induced nuclear reactions experiment, the composition of the targets was determined by fitting the RBS spectra acquired at CTN with the help of the NDF/WiNDF software [14].

Previously, both targets were analysed with the ToF-ERDA technique with a ^{35}Cl beam. The depth profiles obtained by this technique can be seen in Figure 4.1.

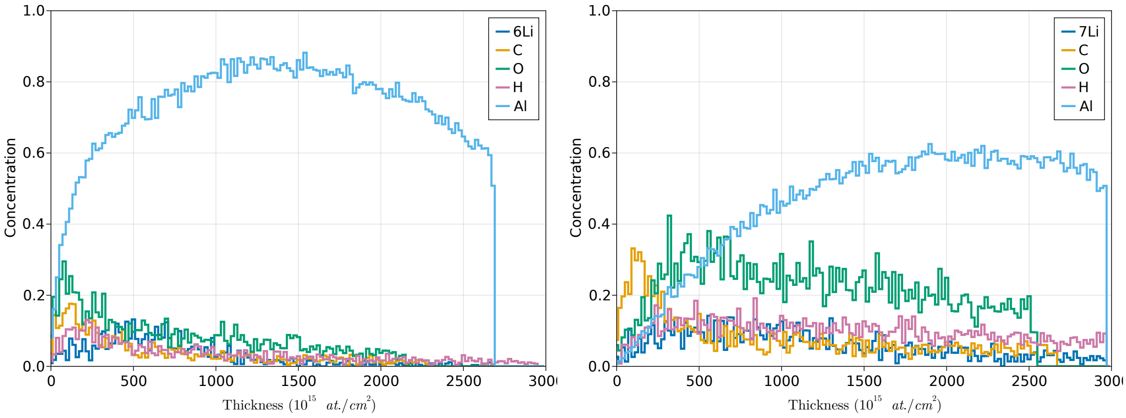

(a) ^{6}Li Target

(b) ^{7}Li Target

Figure 4.1: Depth profiles of the targets obtained by ToF-ERDA with a ^{35}Cl beam

The profiles obtained by ToF-ERDA were then renormalized so that the total elemental concentrations were 100% and number of layers was reduced (maintaining the quantities of each element). These profiles were used to simulate the RBS spectra (acquired with a ^{3}He$^+$ beam). The simulations presented some differences relative to the experimental spectra. For the ^{6}Li target profile, only minor changes had to be made regarding the thickness of some layers.

When simulating the RBS spectra acquired for the ^{7}Li target and using the profile obtained by ToF-ERDA, it was observed that, aside from other minor changes, it would be necessary to add more layers to the profile in order to account for some missing substrate so that the simulated spectra would fit the experimental spectra. Figure 4.2 shows an experimental RBS spectrum and two simulated spectra: one is the simulation performed with the profile determined by ToF-ERDA and the other is the simulation performed with the final profile.

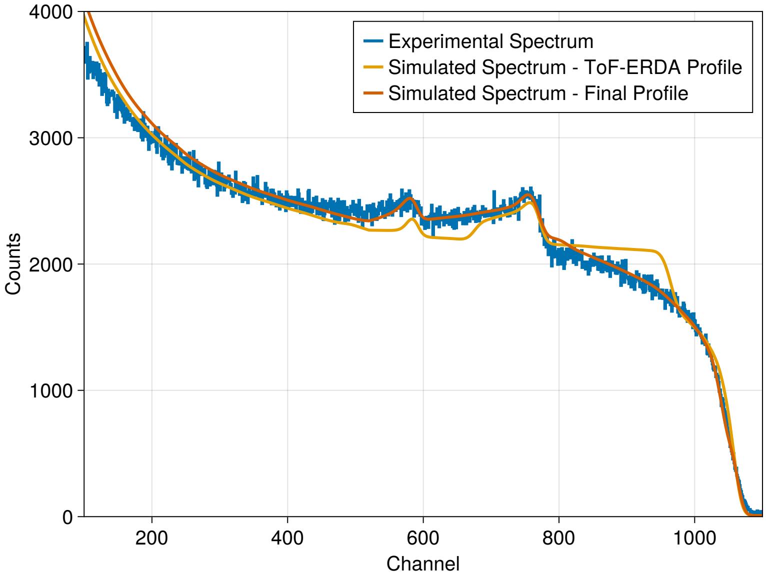

Figure 4.2: Simulated vs Experimental RBS spectrum of the ^{7}Li target

The final elemental depth profiles determined for both targets are presented in Figure 4.3. In Appendix A, the profiles are presented in table form. Note that the difference between the amount of lithium determined by ToF-ERDA and, later, by RBS is within 15% for both targets.

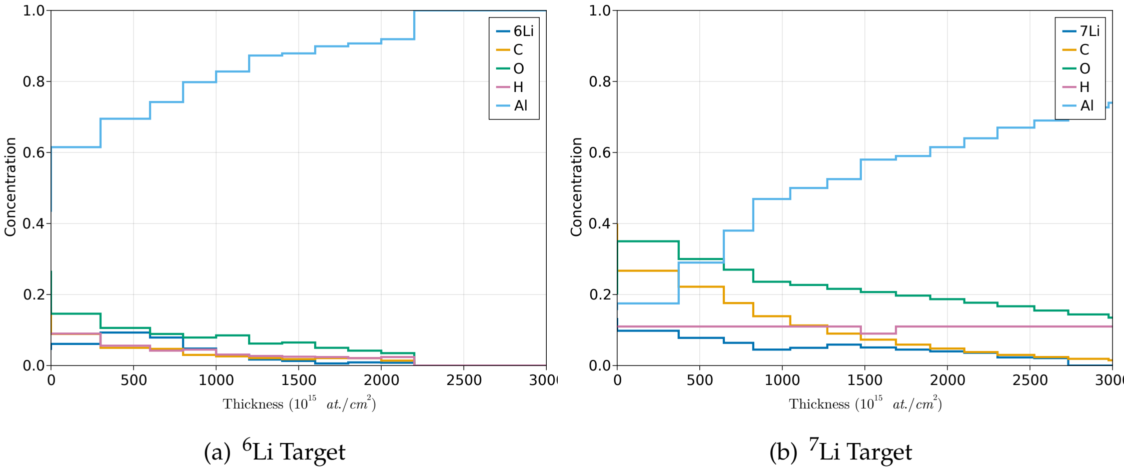

(a) ^{6}Li Target

(b) ^{7}Li Target

Figure 4.3: Final elemental depth profiles determined

4.1.2 Proton Elastic Scattering Reactions

In the proton elastic scattering experiment, the composition of the target was determined by both the simulation of RBS and EBS (Elastic Backscattering Spectrometry) spectra with the help of the SIMNRA software [34].

In this project, some RBS spectra of the target were acquired before the acquisition of the EBS spectra, allowing the characterization of the target before the experiment itself. Similarly to subsection 4.1.1, the amount of Li could not be determined directly. However, in this project, the target was produced by evaporating LiF on top of a silver thin film (see section 3.1.2), so it was considered that the number of atoms of Li is equal to the number of atoms of F (which is a result verified by CTN and other laboratories).

In order to interpret the EBS spectra correctly, some EBS spectra were simulated in SIMNRA for different beam energies and compared with the acquired spectra. Using the profile determined earlier, there were two differences between the simulated and the experimental spectra: the peaks of the simulated spectra were at the right of the corresponding peaks of the experimental spectra and the second peak corresponding to the reaction ^{12}C(p,p)^{12}C was bigger in the experimental spectra than it was in the simulated ones (see Figure 4.5 of Section 4.2.2). Additionally, these differences are larger for spectra acquired later, which led to the conclusion that a small carbon layer was formed on top of the film and got larger every run.

To study the evolution of the carbon layer, some spectra acquired at different times of the experiment were fitted in SIMNRA. Then, the thickness of the carbon layer as a function of the beam energy was studied (spectra acquisition started in the highest energy and ended in the lowest energy). A linear relation between the beam energy and the thickness of the carbon layer was verified, given by the equation:

$$\Delta x_C = -0.2014 * E + 471.78 \tag{4.1}$$

where E is the beam energy in keV, the slope is in units of 10^{15} at./(cm^2 keV) and the intercept is in units of 10^{15} at./cm^2.

The linear relation given by equation (4.1) will be important in section 4.3, where the calculation of the effective energy is explained.

4.2 Peak Identification and Spectra Analysis

In this section, the goal is to interpret the different types of spectrum analysed, by studying the energetics (equations (2.3) and (2.4)) and the kinematics (equation (2.5)) of the different nuclear reactions at play during the experiments.

4.2.1 ^{3}He Induced Nuclear Reactions

In this experiment, two different types of spectra were analysed to determine the excitation functions of the nuclear reactions of interest. Figure 4.4 show an example of each type of spectrum with the identification of each peak, respectively. Both spectra were acquired for a beam energy of E = 2500 keV and a scattering angle of 115°.

In Figure 4.4, some nuclear reactions appear with more than one proton group (the reactions ^{16}O(^{3}He,p$_{2,3,4}$)^{18}F and ^{7}Li(^{3}He,p$_{3,4}$)^{9}Be), because it is not possible to resolve each

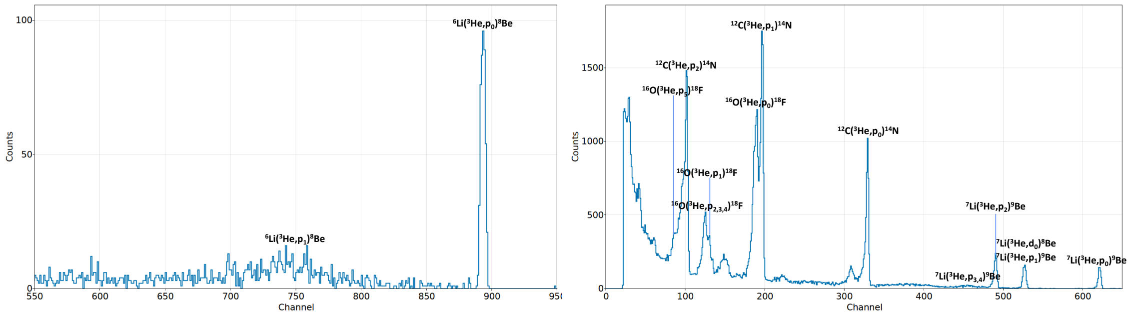

(a) ^{6}Li Target

(b) ^{7}Li Target

Figure 4.4: NRA spectra acquired for E = 2500 keV and θ = 115°

reaction individually. Additionally, in this spectrum (and in higher energy spectra - until approximately 1700 keV), the peaks of reactions ^{7}Li(^{3}He,p$_1$)^{9}Be and ^{7}Li(^{3}He,d$_0$)^{8}Be are overlaid.

4.2.2 Proton Elastic Scattering Reactions

The spectra analysed in this project are simpler to interpret than the ones from section 4.2.1. Figure 4.5 shows the spectrum acquired for a nominal beam energy of 2050 keV and for a scattering angle of 165°, where the 8 peaks that constitute the spectra are identified.

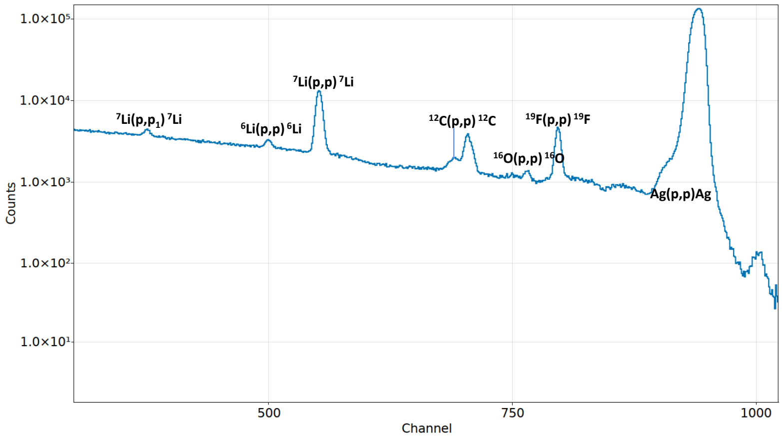

Figure 4.5: EBS spectrum acquired for E = 2050 keV and θ = 165°

4.3 Calculation of the Effective Energy

When performing an experiment which consists of probing a sample with a particle beam (of protons or ^{3}He, for instance), there is a need to control the conditions under which the experiment occurs, such as the energy of the particle beam.

For example, to determine the differential cross section of a nuclear reaction for energy E_0 (and scattering angle θ), the beam energy would be set to E_0 and the spectrum would be acquired as usual. However, the target is not an infinitely thin film, it has depth, so it is necessary to take into account the fact that the element being probed in the material is not exclusively at the surface (when it is at the surface). The nuclear reaction can occur at the surface of the target, where the energy of the incident particle is E_0, or it can occur somewhere inside the sample, where the energy of the particle is smaller than E_0 due to losses in collisions in the material. Therefore, there is a need to correct the energy corresponding to a certain differential cross section value. The corrected energy is usually called effective energy.

The rest of the section will be dedicated to the explanation and comparison of two methods: the half-thickness approximation and an iterative method.

4.3.1 Half-Thickness Approximation

The half-thickness approximation is a coarse method of calculating the effective energy, which works well for thin films, so it was used in the proton elastic scattering experiment.

The basic assumption is that in a layer with an uniform distribution of elements, on average, the nuclear reaction being studied will occur at the point where the particle lost half of the energy that it would lose at the end of the layer. Mathematically, it is calculated as follows:

$$E_{\text{eff}} = E_0 - \frac{\Delta E}{2} \tag{4.2}$$

$$\Delta E = \int \frac{dE}{dx} dx \tag{4.3}$$

For thin targets, it is reasonable to assume that both the stopping power and the cross section are approximately constant throughout the layer. Additionally, thin films can usually be divided in well established layers with approximately uniform distribution of elements in each layer. These factors are what makes this simple method of calculating the effective energy a good approximation, as stated previously.

This approximation can be derived from the iterative method that will be explained in the next section. In fact, the explanation of the iterative method can help understand the assumptions behind this approximation.

4.3.2 Iterative Method

The iterative method of calculating the effective energy is a lot more sofisticated than the half-thickness approximation and is inspired by pages 296-301 of the book “Cauldrons in the Cosmos” by Rolfs [45]. The explanation of this method will be accompanied by visual aids to better help understand the different steps. **Note:** The plots shown in this section are purely schematical, no calculations were made with any numbers for the example, the “results” from certain steps were assumed purely for convenience.

The starting point for this method is an excitation function. Figure 4.6 shows a fictional excitation function with a smooth increasing tendency.

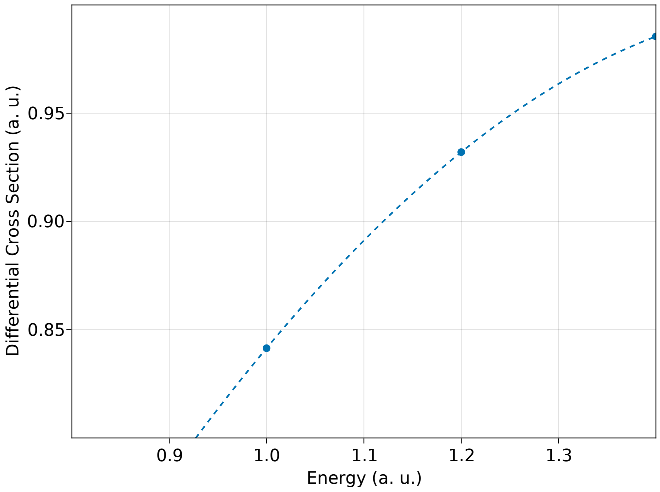

Figure 4.6: Fictional Excitation Function

To calculate the effective energy of a point, for example, the point of beam energy $x = 1.2$, the first step is to determine the minimum energy that, for a certain beam energy, an incident particle can have so that the reaction being studied occurs inside the sample. In this example, it is assumed that the minimum energy is $x = 1.0$. Then, the integral of the excitation function in the interval $[1.0, 1.2]$ is calculated numerically with the trapezoidal rule.

The new effective energy corresponds to the value of x which divides the area under the curve in two equal halves (similar to the determination of a median). In the example, it will be considered for convenience that the new effective energy is $x = 1.1$ (**Note:** By looking at Figure 4.7(a), it is obvious that $x = 1.1$ does not divide the trapeze equally in two halves).

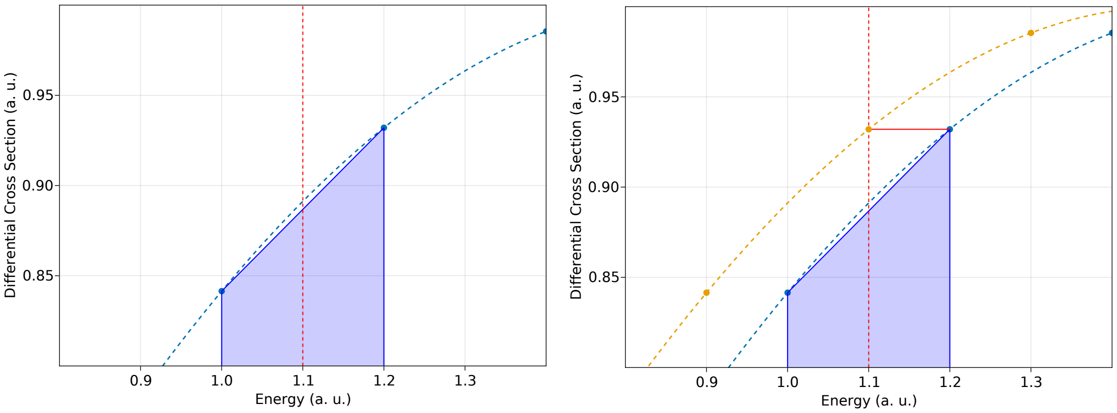

(a) New effective energy

(b) New (fictional) excitation function

Figure 4.7: Representation of the first iteration of the iterative method where a new excitation function (yellow) is generated from the initial excitation function (blue)

This procedure is repeated for every experimental point that constitutes the excitation function. To get the updated excitation function, it is necessary to make a horizontal translation of every point from the initial value of energy to the effective energy value determined for each point. In the example, it was assumed (irrealistically) that each experimental point suffered a horizontal translation of $\Delta x = -0.1$, as it can be seen in Figure 4.7(b). The red line represents the translation of the experimental point where $x = 1.2$.

The determination of the new excitation function concludes the iteration. The iterative process stops if condition (4.4) is met for every experimental point.

$$E_i - E_{i+1} < \text{stop condition} \tag{4.4}$$

where E_i is the energy value of an experimental point in iteration i. In the present work, a stop condition value of 0.01 was assumed.

Imagining that in the example, condition (4.4) is not met, it would be necessary to perform a new iteration. To calculate the new value of effective energy for the same point as before, the interval of integration is still $[1.0, 1.2]$, because $x = 1.0$ and $x = 1.2$ were the minimum and maximum energies with which the reaction being studied occurred in this run. In other words, what moved was the excitation function, not the beam energy. Since that for the new excitation function, the cross section values for $x = 1.0$ and $x = 1.2$ are unknown, they are estimated by applying the “linear approximation” (see Figure 4.8(a)).

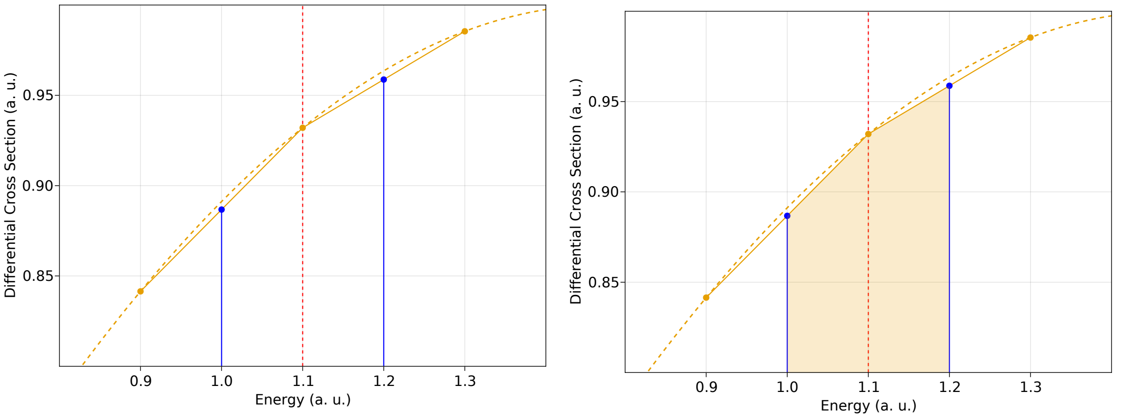

(a) Calculated cross section values for $x = 1.0$ and $x = 1.2$ (by “linear approximation”)

(b) New area under the excitation function in the interval between $x = 1.0$ and $x = 1.2$

Figure 4.8: Representation of the second iteration of the iterative method

After determining the cross section values for $x = 1.0$ and $x = 1.2$, the next step is to calculate the “median” of the excitation function in the interval $[1.0, 1.2]$ as before. Note that it is necessary to take into account the experimental point that is located between the limits of integration in the calculation of the integral, as represented in Figure 4.8(b).

4.3.2.1 Future Developments of the Method

At the time of writing, the iterative method implemented works as described previously, where the depth distribution of the element being probed is assumed constant, which is not always true. In fact, it is not true for the implanted targets of ^{6}Li and ^{7}Li, as discussed in Section 4.1.1.

At the moment, the effective energy E_{eff} is calculated so that:

$$\int_{E_1}^{E_{\text{eff}}} \sigma(\theta, E) dE = \frac{1}{2} \int_{E_1}^{E_0} \sigma(\theta, E) dE \tag{4.5}$$

To take the depth distribution of, for example, ^{7}Li into account, it is necessary to include it into equation (4.5), as shown in equation (4.6).

$$\int_{E_1}^{E_{\text{eff}}} \sigma(\theta, E) N_{\text{Li}}(E) dE = \frac{1}{2} \int_{E_1}^{E_0} \sigma(\theta, E) N_{\text{Li}}(E) dE \tag{4.6}$$

The first thing to notice is that if $N_{\text{Li}}(E)$ is constant, then equation (4.6) becomes equation (4.5) (and if the excitation function is also constant, this method obtains the same result as the half-thickness approximation).

The second thing to notice is that $N_{\text{Li}}(E)$ is a function of the energy, but in Section 4.1 presented are always a function of the sample depth x, $N_{\text{Li}}(x)$. Therefore, an extra step of determining the depth distribution as a function of energy is needed for every differential cross section point.

4.3.3 Comparison of both methods

In this subsection, a brief comparison between both methods will be made, in which the depth distribution is not accounted for.

In the proton elastic scattering experiment, the method of choice was the half-thickness approximation, because the target used was a thin film. Therefore, to compare the two methods, an excitation function determined in the ^{3}He-induced nuclear reactions was subjected to both of them, specifically the one for the ^{7}Li(^{3}He,p$_{0}$)^{9}Be reaction for a scattering angle of 115°.

For the half-thickness approximation, the average difference between the initial energy and the effective energy of a cross section point is 5 keV. For the iterative method, the average difference is 20 keV, i.e. 4 times the difference for the half-thickness approximation.

In conclusion, because of the difference of the effective energies calculated and since the iterative method takes into account the differential cross sections determined for the calculations, the iterative method was chosen to determine the effective energies of the points of the excitation functions determined for nuclear reaction induced by ^{3}He.

4.4 Uncertainty Analysis

Uncertainty analysis is one of the most important parts of any experimental work. The uncertainty of the differential cross sections determined was calculated by propagation of uncertainty (equation (4.7)), such as all the physical quantities measured indirectly (Appendix B contains the specific formulas used to calculate uncertainties via propagation of uncertainty).

$$u(Z) = \sqrt{\left(\frac{\partial Z}{\partial x_0}\right)^2 (u(x_0))^2 + \left(\frac{\partial Z}{\partial x_1}\right)^2 (u(x_1))^2 + \ldots} \tag{4.7}$$

where Z is a physical quantity that depends on other physical quantities x_0, x_1, etc. The propagation of uncertainty formula assumes that the uncertainties of the different physical quantities are uncorrelated.

To calculate the uncertainties of the final differential cross sections, uncertainties of various parameters have to be determined (see equations (2.7) and (2.9)). Table 4.1 presents the uncertainties considered for the measurements, where a distinction between statistical and systematic uncertainties is made.

Table 4.1: Uncertainty budget for the measurements

Uncertainty Source	Amount
Statistical	
Counting Statistics	1.0% - 37.8%
Areal Density of the Implanted Targets	*15%
Accumulated Charge	3%
Systematic	
Energy	5 - 11 keV
Angle of Detection	2°
Stopping Power	5%
Detector Solid Angle	3%

The uncertainty of the areal density of elements in the targets is used directly in the calculation of the uncertainty of the cross sections (in the ^{3}He-induced reactions experiment), since the areal density is a parameter of equation (2.7). In the proton elastic scattering experiment, it is used to calculate the uncertainty of the stoichiometric factor n (see equation (2.8)). Note that the uncertainty of the areal densities is marked with a "*", since the current values are an estimation susceptible to change after some normalization measurements.

As for the areal densities, the uncertainty of the accumulated charge is used to calculate the uncertainty of the cross sections directly, in the ^{3}He-induced reactions experiment.

The uncertainty of the energy is used to calculate the uncertainty of the Rutherford cross sections of silver that are used to calculate the final differential cross sections in the proton elastic scattering experiment. But, more importantly, the uncertainty of the energy is in itself an uncertainty in the x-axis of a differential cross section point.

The remaining systematic uncertainties are well known uncertainties determined in previous works. The angle of detection is used to calculate the Rutherford cross sections of silver, similarly to the energy. The stopping power is used to calculate the effective energy. Finally, the solid angle of the detector is used to calculate the differential cross sections directly (equation (2.7)).

4.4.1 Counting Statistics Uncertainty

From the sources of uncertainty displayed in Table 4.1, counting statistics is the only one left to discuss.

It is known that the arrival of particles to the detector can be described as a poissonian process, in which the standard deviation of a poisson distribution is given by $\sqrt{\lambda}$ (and the average of the distribution given by λ). If the number of events detected Y is assumed to be the average, then:

$$u(Y) = \sqrt{Y} \tag{4.8}$$

In many cases, it was necessary to remove the background from the spectra in order to determine the net yield (Y_{net}) - in opposition to the gross (total) yield (Y_{gross}). In those cases, the uncertainty of counting statistics was calculated as follows:

$$u(Y_{\text{net}}) = \sqrt{(Y_{\text{gross}} + Y_{\text{bkg}}) * \frac{\text{width}}{2}} \tag{4.9}$$

$$Y_{\text{bkg}} = Y_{\text{gross}} - Y_{\text{net}} \tag{4.10}$$

where the width of the region of interest (ROI) was considered [43].

From Table 4.1, it is possible to see that the uncertainty of counting statistics can range from 1.0% to 37.8%. The large disparity between the values can be explained essentially by two factors:

- The first factor is statistical: if more counts are acquired, then the uncertainty is smaller, in percentage;
- The second factor is the signal/background ratio: by equation (4.9) it becomes evident that the bigger the background is the bigger the counting statistics uncertainty will be.

4.4.2 Internal and External Uncertainties

In the proton elastic scattering experiment, the differential cross sections for the ^{19}F(p,p)^{19}F reaction was determined by prof. Javier Ferrer, from Seville University, and by the author of the current work in parallel (with exchange of ideas along the way).

Since both analysis of the data were performed with different methods, the results were slightly different, so the final excitation function for this nuclear reaction was determined by averaging the results obtained from both methods.

To calculate the uncertainties of the final excitation function, it was necessary to take into account the uncertainties determined by both methods and the differences between results. In data points where the results obtained from both methods are similar, the uncertainties calculated from these methods (called internal uncertainties) prevail over the difference of results. On the other hand, if the difference between results (external uncertainty) is larger than the internal uncertainties, the external uncertainty is of more importance. Therefore, the uncertainties from the data points of the final excitation function for the nuclear reaction ^{19}F(p,p)^{19}F were determined by equation (4.11).

$$u\left(\sigma(\theta)_{\text{Final}}\right) = \max\left(u_{\text{int}_{\text{Lisbon}}}, u_{\text{int}_{\text{Seville}}}, u_{\text{ext}}\right) \tag{4.11}$$

4.5 Results and Discussion

In this section, the results from both experiments will be presented and a comparison of these with the literature will be made.

4.5.1 ^{3}He Induced Nuclear Reactions

The excitation functions determined for ^{3}He induced nuclear reactions in ^{6}Li and ^{7}Li in this work for scattering angles of 115°, 125°, 135°, 145°, 155° and 165° are shown in Figure 4.9 (the figure does not show the error bars on purpose in order to keep it as clean as possible - the uncertainties calculated can be seen in Appendix C). The first aspect to notice is the clear angular dependency in the differential cross sections. The nuclear reactions ^{7}Li(^{3}He,p$_i$)^{9}Be ($i = 0, 2$) and ^{7}Li(^{3}He,d$_0$)^{8}Be appear to be isotropic for low energies and anisotropic for beam energies greater than 1400 keV, approximately. It is also possible to note a presence of a resonance at ≈ 2100 keV for the ^{7}Li(^{3}He,p$_2$)^{9}Be reaction excitation functions.

The differential cross section values range from 0.17 mb/sr to 2.49 mb/sr and their relative uncertainties from 10.3% to 35.3%.

Note that there is not an excitation function for the reaction ^{7}Li(^{3}He,p$_{3,4}$)^{9}Be for scattering angle of 155° due to not enough resolution of the detector which made limiting the peak corresponding to the reaction a difficult task. Additionally, it was not possible to determine differential cross sections for the nuclear reaction ^{7}Li(^{3}He,p$_1$)^{9}Be for two reasons: at high energies, the peak corresponding to the reaction overlaps with the peak of the ^{7}Li(^{3}He,d$_0$)^{8}Be reaction; at low energies, it is possible to identify the existence of the peak but it is difficult to define its limits. Lastly, despite the identification of the ^{6}Li(^{3}He,p$_1$)^{8}Be being possible, it was difficult to determine where the peak started and ended exactly, for which excitation functions for this reaction were not determined.

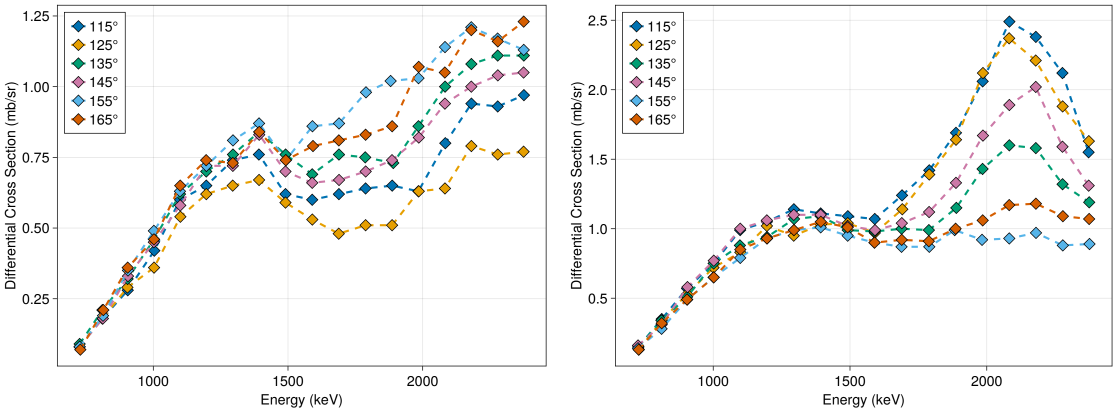

(a) ^{7}Li(^{3}He,p$_{0}$)^{9}Be (b) ^{7}Li(^{3}He,p$_{2}$)^{9}Be

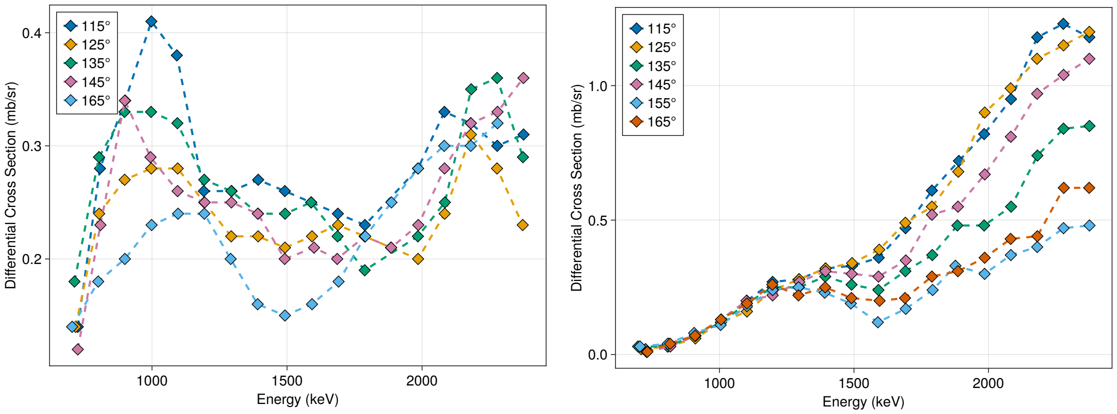

(c) ^{7}Li(^{3}He,p$_{3,4}$)^{9}Be (d) ^{7}Li(^{3}He,d$_{0}$)^{8}Be

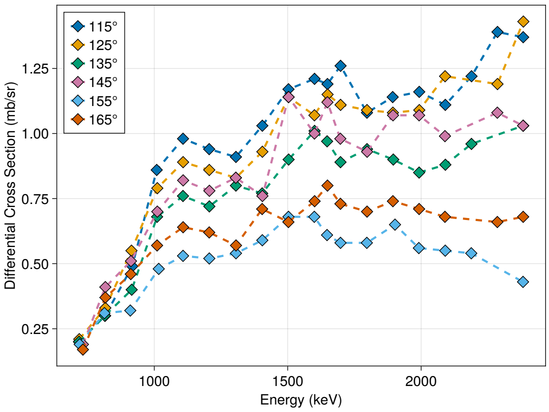

(e) ^{6}Li(^{3}He,p$_{0}$)^{8}Be

Figure 4.9: Excitation functions for nuclear reactions induced by ^{3}He in lithium

In order to compare some of the obtained results with the literature, the plots of Figure 4.10 were made. Contrary to Figure 4.9, in Figure 4.10 the uncertainties calculated in the current work are shown in error bars (although there are no error bars for the datasets from previous works, so that the plots are not overloaded).

Each subfigure in Figure 4.10 shows at least one of the excitation functions determined in the present work and all of the excitation functions determined for the same nuclear reaction and whose angle of detection is between $\theta - 5°$ and $\theta + 5°$ (the difference between the angles of detection of different datasets can be up to 25° when there is more than one excitation function determined in this work in a subfigure). Since, previously, it was concluded that there is an angular dependency in the differential cross sections, some discrepancies between datasets can be explained by this angular dependency.

From observing Figures 4.10(a), 4.10(b), 4.10(c), 4.10(d) and 4.10(e), it is possible to conclude that the datasets from D. P. Rath's work [23] does not agree with any of the remaining datasets. Furthermore, each dataset has only 4 points.

In Figure 4.10(a), there is a good agreement between the experimental results from the current work (θ = 115°) and data from Y. C. Lru [19] (θ = 120°). This dataset from Y. C. Lru [19] also has a good agreement with the excitation function determined by I. I. Bondouk [20] for θ = 120°, as seen in Figure 4.10(b), although for energies lower than 1600 keV the cross sections determined in the present work for θ = 115°, 125° differ from I. I. Bondouk's data [20].

Similarly, in Figure 4.10(c), the shape of the excitation function determined in the present work (θ = 135°) is similar to I. I. Bondouk's data [20] (θ = 130°) in the energy interval from 1500 keV to 2500 keV, but it is different for energies lower than 1500 keV. In the lower energy region, the shape of the excitation functions determined in this work for the ^{7}Li(^{3}He,p$_0$)^{9}Be reaction show a resonance at 1400 keV, while the datasets from I. I. Bondouk [20] show a smooth increase of the cross section with the energy.

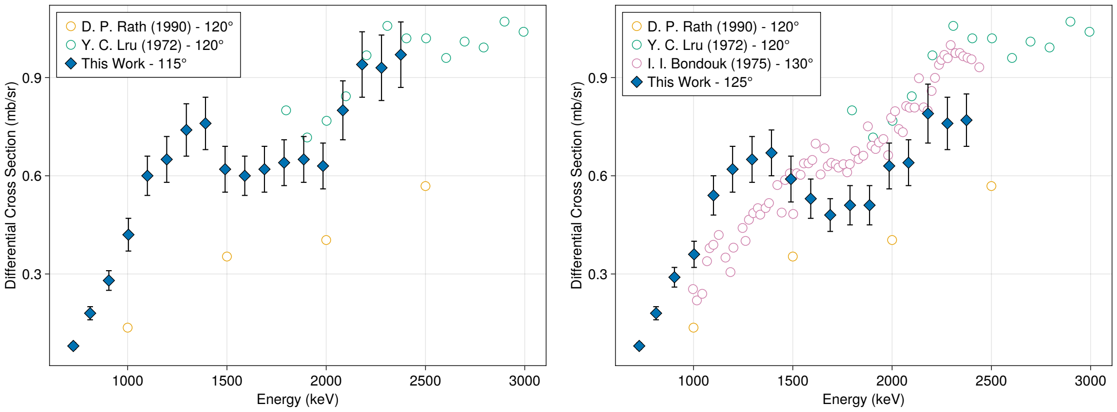

(a) ^{7}Li(^{3}He,p$_0$)^{9}Be, θ = 115° [19, 23]

(b) ^{7}Li(^{3}He,p$_0$)^{9}Be, θ = 125° [19, 20, 23]

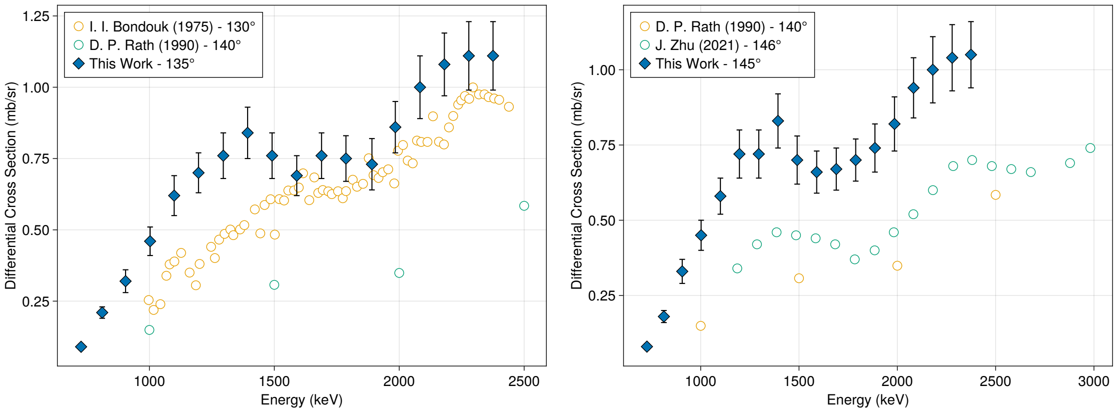

(c) ^{7}Li(^{3}He,p$_{0}$)^{9}Be, $\theta = 135°$ [20, 23]

(d) ^{7}Li(^{3}He,p$_{0}$)^{9}Be, $\theta = 145°$ [23, 24]

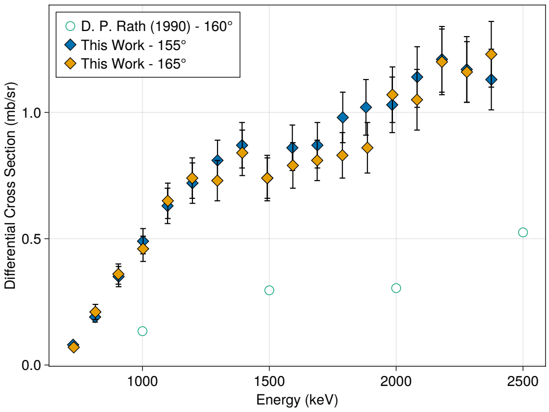

(e) ^{7}Li(^{3}He,p$_{0}$)^{9}Be, $\theta = 155°, 165°$ [23]

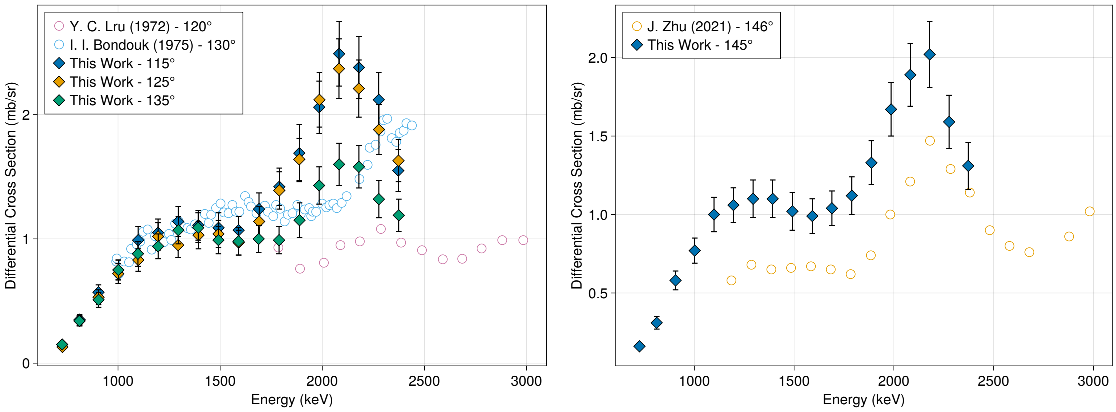

(f) ^{7}Li(^{3}He,p$_{2}$)^{9}Be, $\theta = 115°, 125°, 135°$ [19, 20]

(g) ^{7}Li(^{3}He,p$_{2}$)^{9}Be, $\theta = 145°$ [24]

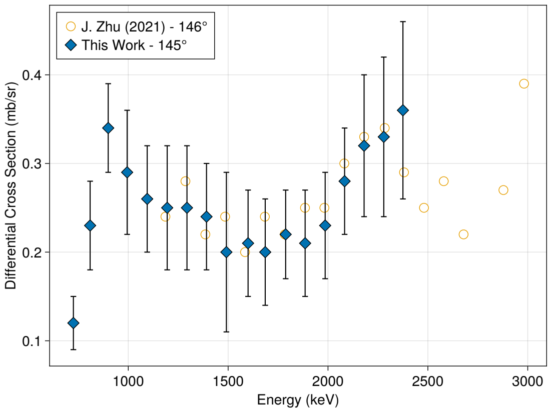

(h) ^{7}Li(^{3}He,p$_{3,4}$)^{9}Be, θ = 145° [24]

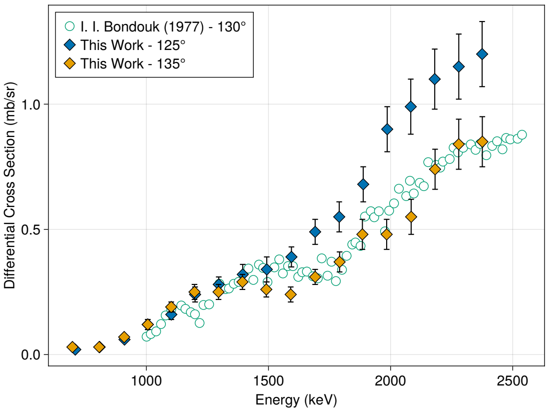

(i) ^{7}Li(^{3}He,d$_0$)^{8}Be, θ = 125°, 135° [21]

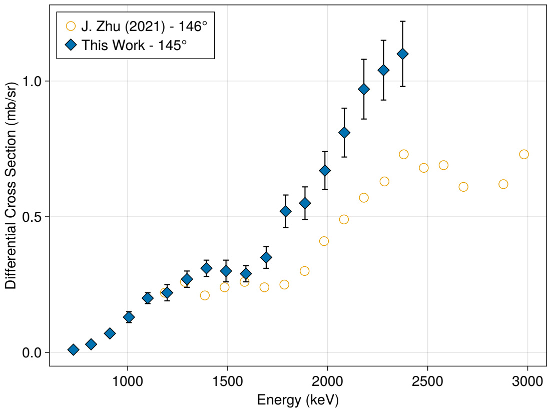

(j) ^{7}Li(^{3}He,d$_0$)^{8}Be, θ = 145° [24]

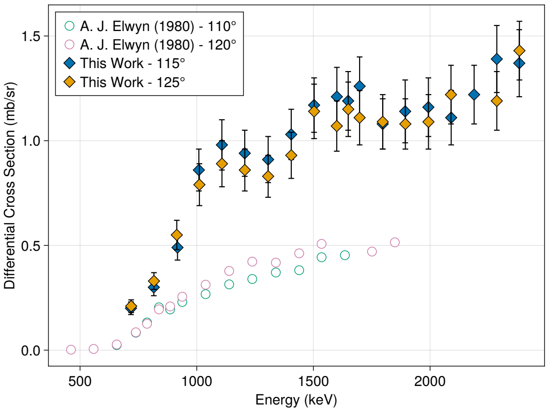

(k) ^{6}Li(^{3}He,p$_0$)^{8}Be, θ = 115°, 125° [22]

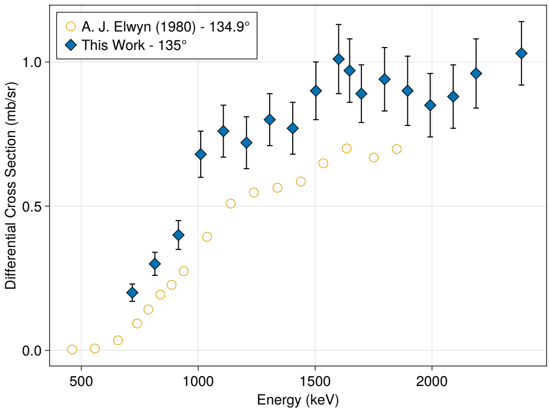

(l) ^{6}Li(^{3}He,p$_0$)^{8}Be, θ = 135° [22]

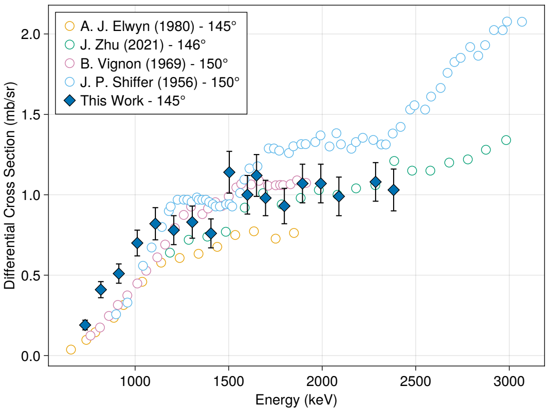

(m) ^{6}Li(^{3}He,p$_0$)^{8}Be, θ = 145° [17, 18, 22, 24]

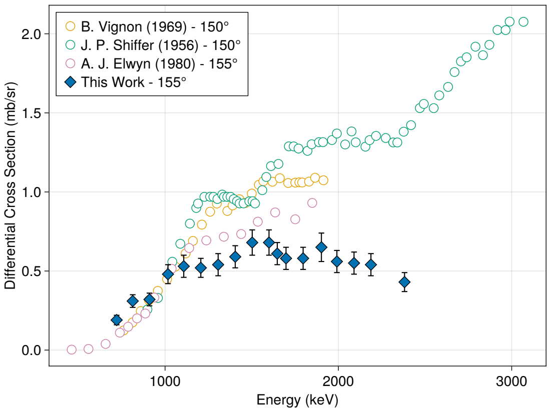

(n) $^{6}Li(^{3}He,p_{0})^{8}Be$, $\theta = 155°$ [17, 18, 22]

Figure 4.10: Comparison of the excitation functions obtained in the current work for nuclear reactions induced by ^{3}He in lithium for different angles with datasets from other authors

By comparing the excitation functions determined by this work for the nuclear reactions $^{7}Li(^{3}He,p_{0})^{9}Be$ and $^{7}Li(^{3}He,p_{2})^{9}Be$ and the ones determined by J. Zhu [24], in Figures 4.10(d) and 4.10(g), it seems that the shape of the excitation functions are identical, but that one of them can be obtained from the other by a vertical translation. It is possible that a systematic error might be the origin of the difference between the datasets.

Still comparing with J. Zhu's work [24], but now for the $^{7}Li(^{3}He,p_{3,4})^{9}Be$ reaction, it is possible to conclude, from Figure 4.10(h), that there is a very good agreement between the cross sections determined in both works.

In Figure 4.10(f), there is a good agreement between the excitation functions determined in the present work for the nuclear reaction $^{7}Li(^{3}He,p_{2})^{9}Be$ and the excitation function determined by I. I. Bondouk [20] for lower energies. However, the resonance that exists in the energy interval between 1800 keV and 2500 keV in the excitation functions resultant from this work is not present in Bondouk's work [20].

In Figure 4.10(i), there is a very good agreement between the excitation function determined in this work for a scattering angle of 135° and the excitation function determined by I. I. Bondouk [21]. Regarding the excitation function determined for a scattering angle of 125°, it differs from the other excitation functions for higher energies, starting in 1500 keV.

The two excitation functions presented in Figure 4.10(j) for the nuclear reaction $^{7}Li(^{3}He,d_{0})^{8}Be$ ($\theta = 145°$) do not agree between each other. The same conclusion can be drawn when comparing the excitation functions obtained in the present work for the $^{6}Li(^{3}He,p_{0})^{8}Be$ reaction with the differential cross sections determined by [22] that are shown in Figures 4.10(k) and 4.10(l).

In Figure 4.10(m), the obtained results seem to validate the excitation function determined by J. Zhu [24], with the exception of some outliers.

Lastly, in Figure 4.10(n), the excitation function determined in the current work does not agree with the literature.

In conclusion, in this work, excitation function for nuclear reactions induced by ^{3}He in lithium were determined, expanding the available data on these reactions for different detection angles and energy ranges. Additionally, it was possible to perform a comparison with the literature. Despite the discrepancies between the excitation functions determined in this work and the ones from previous works, the methodology followed to produce the new data is a factor that give confidence to the obtained results. Since the methodology followed for this project was similar to the one followed in the proton elastic scattering experiment, the results shown in the next subsection contribute to validate it.

4.5.2 Proton Elastic Scattering Reactions

As mentioned in Section 1.6, the goal of this project was to determine the excitation functions for the nuclear reactions ^{6}Li(p,p)^{6}Li, ^{7}Li(p,p)^{7}Li and ^{19}F(p,p)^{19}F.

Starting in the ^{19}F(p,p)^{19}F reaction, Figure 4.11 shows the final excitation function determined in the present work, an evaluation performed by A. F. Gurbich's SigmaCalc [16] for beam energies lower than 1750 keV and experimental differential cross sections for beam energies greater than 1490 keV determined by V. Paneta [46]. The differential cross section values range from 0.30 rr and 2.83 rr and their relative uncertainties from 4.9% to 14.5%.

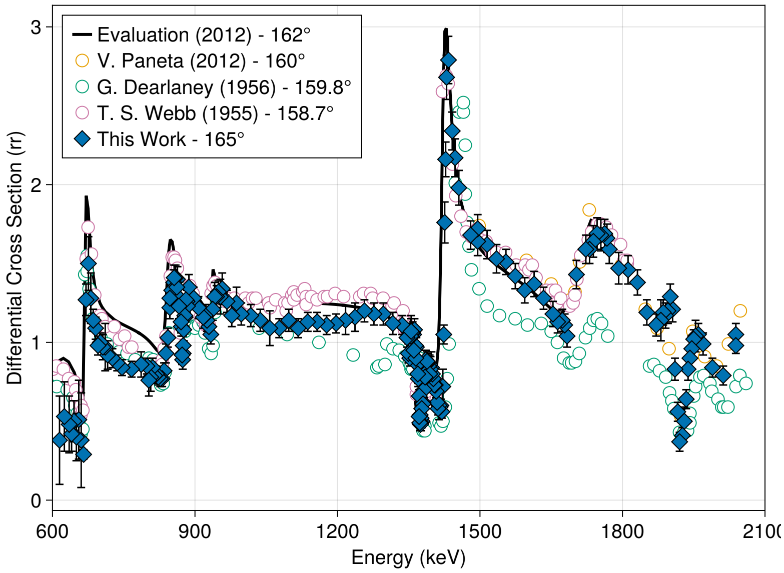

Figure 4.11: ^{19}F(p,p)^{19}F excitation function

Comparing the experimental data with Gurbich's evaluation, it can be inferred that, in a general way, the data agrees with the evaluation, especially in the 800 - 1000 keV and the 1300 - 1750 keV zones (in this last zone in particular, the narrow resonance is really well defined). However, in the 1000 - 1300 keV zone there is a clear discrepancy between the experimental data and the evaluation, since the data appears to have a small concavity facing up, whereas in the same energy zone the evaluation shows an approximately constant cross section. For energies below 800 keV, there is a considerable difference between experiment and theory, where the shape of the excitation function is similar to the shape of the evaluation, but the values of cross section differ by about 0.25 rr.

When comparing the results from this work with V. Paneta's dataset, it is possible to conclude that there is a good agreement between the results from both experiments.

Regarding the ^{7}Li(p,p)^{7}Li reaction, the differential cross sections obtained in the experiment are presented in Figure 4.12, along with experimental data from other authors [32, 33] so that comparison can be made. The differential cross section values range from 0.07 rr and 37.93 rr and with an average relative uncertainty of 14.2%. From Figure 4.12, it is possible to conclude that the experimental data from this work agrees with previous cross section measurements for this nuclear reaction.

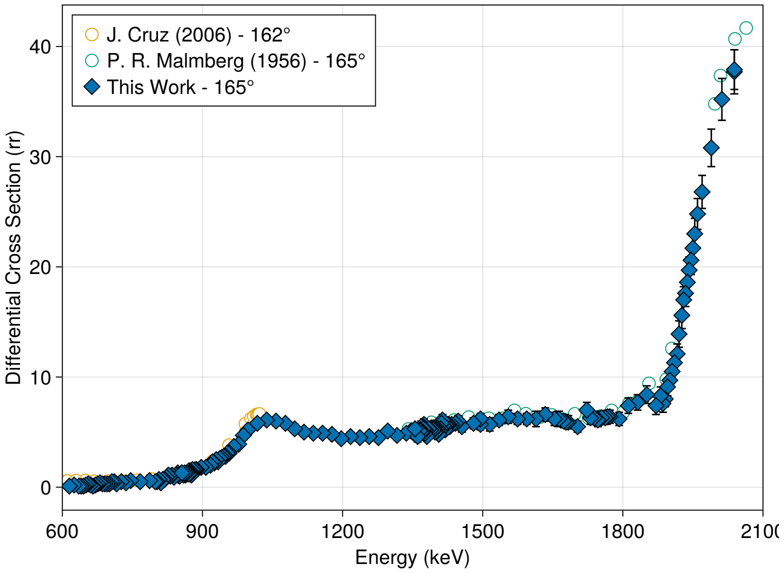

Figure 4.12: ^{7}Li(p,p)^{7}Li excitation function

Lastly, Figure 4.13 shows the excitation function for the ^{6}Li(p,p)^{6}Li determined in the present work, along with experimental data from U. Fasoli [31]. The differential cross section values range from 45.23 mb/sr and 155.34 mb/sr and with an average relative uncertainty of 25.8%.

A considerable dispersion in the results obtained in this work is noticeable. This dispersion can be explained by the presence of low quantities of ^{6}Li in the target, whereby a small change in the net yield causes a significant change in the cross section. Despite the dispersion of the results and the large uncertainties being responsible for these results not improving upon previous work, the differential cross sections determined for the

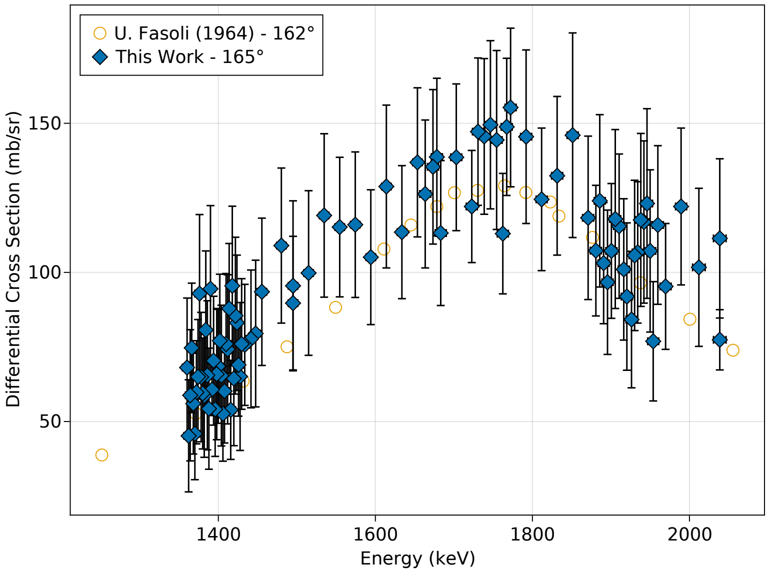

Figure 4.13: ^{6}Li(p,p)^{6}Li excitation function

^{6}Li(p,p)^{6}Li reaction are useful, since it is able to confirm results from the literature for this reaction.

5

CONCLUSIONS AND FUTURE PROSPECTS

In this work, the results for ^{3}He induced nuclear reactions in lithium experiment were presented and discussed, as well as the determined excitation functions for the proton elastic reactions in ^{6}Li, ^{7}Li and ^{19}F.

For the ^{3}He induced reactions experiment, differential cross sections were measured for the nuclear reactions ^{7}Li(^{3}He,p$_i$)^{9}Be ($i = 0, 2, 3, 4$), ^{7}Li(^{3}He,d$_0$)^{8}Be and ^{6}Li(^{3}He,p$_0$)^{8}Be in the 800 keV to 2500 keV energy range and at angles between 115° and 165° with a 10° step. The cross sections vary between 0.17 mb/sr and 2.49 mb/sr, with uncertainties between 10.3% and 35.3%. The excitation functions obtained present a clear angular dependency, especially for higher energies. The obtained results were compared with the literature. From the comparison, two observations should be highlighted: the first one is that for the ^{7}Li(^{3}He,p$_2$)^{9}Be reaction with detection angles of 115°, 125° and 135°, the excitation functions determined in the present work show the existence of a resonance at $\approx$ 2100 keV, which is not present in the dataset from I. I. Bondouk [20]; the other is that, when comparing the cross sections determined in this work for $\theta = 145°$ with the ones measured by J. Zhu [24] for $\theta = 146°$, it is possible to note similarities in the features of the excitation functions determined by both works, but the values of the cross sections differ for some of them. As future work, some new measurements for these nuclear reactions will be performed with a thin LiF target to confirm the current results (and to decrease the uncertainty around the areal densities of Li in the implanted targets), although these measurements are not expected to have a big impact on the results obtained in this work. Additionally, it is expected that more laboratories involved in CRP F11023 (Section 1.4) make new cross section measurements for the same nuclear reactions so that more data is available to compare and discuss the results.

For the proton elastic scattering experiment, differential cross sections were measured for the reactions ^{19}F(p,p)^{19}F, ^{7}Li(p,p)^{7}Li and ^{6}Li(p,p)^{6}Li in the 620 keV to 2050 keV energy range and at a scattering angle of 165°. The obtained results were compared with the literature. In the ^{19}F(p,p)^{19}F reaction, the one that motivated this experiment, the results show a good agreement with Gurbich's evaluation [16], except in some energy zones, as discussed in Section 4.5.2, and with the excitation function determined by V. Paneta [46].

The differential cross sections for the remaining reactions show a good agreement with the literature, despite the high uncertainties obtained for the ^{6}Li(p,p)^{6}Li reaction. In this experiment, the results are final.

Lastly, the obtained results from both experiments are expected to be published in two distinct papers summarizing the work done for both projects in order to make them available for the scientific community and at the database IBANDL.

BIBLIOGRAPHY

[1] J. M. Lourenço. *The NOVAthesis LaTeX Template User's Manual*. NOVA University Lisbon. 2021. URL: https://github.com/joaomlourenco/novathesis/raw/main/template.pdf (cit. on p. ii).

[2] D. Gielen et al. "The role of renewable energy in the global energy transformation". In: *Energy Strategy Reviews* 24 (2019-04), pp. 38–50. ISSN: 2211467X. DOI: 10.1016/j.esr.2019.01.006. URL: https://linkinghub.elsevier.com/retrieve/pii/S2211467X19300082 (cit. on p. 1).

[3] P. Kite and A. Richardson. "The Promise of Nuclear Fusion". In: *PAM Review Energy Science & Technology* 1 (2014), pp. 43–69. DOI: 10.5130/pamr.v1i0.1385 (cit. on p. 1).

[4] C. Vítor. "Determination of the excitation function for nuclear reactions in beryllium induced by helium-3". NOVA School of Science and Technology, 2021. URL: http://hdl.handle.net/10362/134613 (cit. on p. 1).

[5] ITER. *ITER - the way to new energy*. URL: https://www.iter.org/ (cit. on p. 1).

[6] Y. Hirooka. "A review of plasma wall boundary effects on core confinement and lithium applications to boundary-controlled magnetic fusion experiments". In: *Fusion Engineering and Design* 85 (6 2010-11), pp. 838–846. ISSN: 09203796. DOI: 10.1016/j.fusengdes.2010.04.025. URL: https://linkinghub.elsevier.com/retrieve/pii/S0920379610001663 (cit. on p. 1).

[7] A. de Castro, P. Valson, and F. Tabarés. "Hydrogen retention studies on lithiated tungsten exposed to glow discharge plasmas under varying lithiation environments using Thermal Desorption Spectroscopy and mass spectrometry". In: *Fusion Engineering and Design* 117 (2017-04), pp. 212–216. ISSN: 09203796. DOI: 10.1016/j.fusengdes.2016.10.011. URL: https://linkinghub.elsevier.com/retrieve/pii/S092037961630669X (cit. on p. 1).

[8] V. A. Evtikhin et al. “Lithium divertor concept and results of supporting experiments”. In: *Plasma Physics and Controlled Fusion* 44 (6 2002-06), pp. 955–977. ISSN: 0741-3335. DOI: `10.1088/0741-3335/44/6/322`. URL: `https://iopscience.iop.org/article/10.1088/0741-3335/44/6/322` (cit. on p. 1).

[9] M. Rubel. “Fusion Neutrons: Tritium Breeding and Impact on Wall Materials and Components of Diagnostic Systems”. In: *Journal of Fusion Energy* 38 (3-4 2019-08), pp. 315–329. ISSN: 0164-0313. DOI: `10.1007/s10894-018-0182-1`. URL: `http://link.springer.com/10.1007/s10894-018-0182-1` (cit. on p. 2).

[10] N. Barradas et al. “Determination of the 9Be(3He,pi)11B (i=0,1,2,3) cross section at 135° in the energy range 1-2.5MeV”. In: *Nuclear Instruments and Methods in Physics Research Section B: Beam Interactions with Materials and Atoms* 346 (2015-03), pp. 21–25. ISSN: 0168583X. DOI: `10.1016/j.nimb.2015.01.037`. URL: `https://linkinghub.elsevier.com/retrieve/pii/S0168583X15000506` (cit. on p. 3).

[11] M. Mayer et al. “Ion beam analysis of fusion plasma-facing materials and components: facilities and research challenges”. In: *Nuclear Fusion* 60 (2 2020-02), p. 025001. ISSN: 0029-5515. DOI: `10.1088/1741-4326/ab5817`. URL: `https://iopscience.iop.org/article/10.1088/1741-4326/ab5817` (cit. on p. 3).

[12] IAEA. *Development and Application of Ion Beam Techniques for Materials Irradiation and Characterization relevant to Fusion Technology*. URL: `https://www.iaea.org/projects/crp/f11023` (cit. on p. 3).

[13] J. F. Ziegler, M. D. Ziegler, and J. P. Biersack. “SRIM–The stopping and range of ions in matter (2010)”. In: *Nuclear Instruments and Methods in Physics Research Section B: Beam Interactions with Materials and Atoms* 268.11-12 (2010), pp. 1818–1823. DOI: `10.1016/j.nimb.2010.02.091` (cit. on p. 4).

[14] N. Barradas, C. Jeynes, and R. Webb. “Simulated annealing analysis of Rutherford backscattering data”. In: *Applied Physics Letters* 71.2 (1997), pp. 291–293. DOI: `10.1063/1.119524` (cit. on pp. 4, 20).

[15] IAEA. *IBANDL - Ion Beam Analysis Nuclear Data Library*. URL: `https://www-nds.iaea.org/exfor/ibandl.htm` (cit. on pp. 4, 6).

[16] A. Gurbich. “SigmaCalc recent development and present status of the evaluated cross-sections for IBA”. In: *Nuclear Instruments and Methods in Physics Research Section B: Beam Interactions with Materials and Atoms* 371 (2016), pp. 27–32. DOI: `10.1016/j.nimb.2015.09.035` (cit. on pp. 4, 36, 39).

[17] J. Schiffer et al. “Study of the Reaction Mechanism for (He 3, p) Reactions with Li 6, B 10, and C 13”. In: *Physical Review* 104.4 (1956), p. 1064. DOI: `10.1103/PhysRev.104.1064` (cit. on pp. 4, 5, 34, 35).

[18] B. Vignon et al. "Étude des réactions 6Li(3He, p) et 6Li(3He, p$\alpha\alpha$) en dessous de 2 MeV". In: *Journal de Physique* 30 (1969), pp. 11–12. DOI: 10.1051/jphys:019690030011-12091300Ãŕ. URL: http://dx.doi.org/10.1051/jphys:0196900300110-12091300 (cit. on pp. 4, 5, 34, 35).

[19] Y. C. Lru. "Helium-3 Induced Reaction on Li at Bombarding Energies of 2.2 to 3.2 MeV". In: *Chinese Journal of Physics* 10 (1972), pp. 76–83. URL: https://api.semanticscholar.org/CorpusID:116324461 (cit. on pp. 4, 5, 32, 33).

[20] I. Bondouk et al. "An experimental investigation of the reactions 7Li(3He, p0)9Be and 7Li(3He, p2)9Be in the 3He energy range of 1.0 to 2.5 MeV". In: *Revue Roumaine de Physique* 20.10 (1975), pp. 1095–1098. URL: https://digilib.nipne.ro/colectii/files/original/3046e0e6c7b8d57bd72fea01b6e26de02e51fd1c.pdf#page=88 (cit. on pp. 4, 5, 32, 33, 35, 39).

[21] I. Bondouk and S. Saad. "Investigation of the reaction Li7(He3, d0)Be8 in the He3 energy range of 1.0 to 2.5 MeV". In: *Atomkernenergie* 29.4 (1977), pp. 270–271 (cit. on pp. 4, 5, 34, 35).

[22] A. J. Elwyn et al. "Cross sections for the 6Li(3He,p) reaction at energies below 2 MeV". In: *Physical Review C* 22 (4 1980-10), pp. 1406–1419. ISSN: 0556-2813. DOI: 10.1103/PhysRevC.22.1406. URL: https://link.aps.org/doi/10.1103/PhysRevC.22.1406 (cit. on pp. 4, 5, 34, 35).

[23] D. Rath et al. "7Li(3He, p)9Be Reaction and primordial nucleosynthesis". In: *Nuclear Physics A* 515 (2 1990-08), pp. 338–348. ISSN: 03759474. DOI: 10.1016/0375-9474(90)90371-R. URL: https://linkinghub.elsevier.com/retrieve/pii/037594749090371R (cit. on pp. 4, 5, 32, 33).

[24] J. Zhu et al. "Differential cross sections for 7Li(3He,p0 4)9Be, 7Li(3He,d0)8Be and 6Li(3He,p0)8Be from 1.2 to 3 MeV". In: *Nuclear Instruments and Methods in Physics Research Section B: Beam Interactions with Materials and Atoms* 494-495 (2021-05), pp. 23–28. ISSN: 0168583X. DOI: 10.1016/j.nimb.2020.12.014. URL: https://linkinghub.elsevier.com/retrieve/pii/S0168583X2030522X (cit. on pp. 4, 5, 33–36, 39).

[25] A. Gurbich. "Evaluated differential cross-sections for IBA". In: *Nuclear Instruments and Methods in Physics Research Section B: Beam Interactions with Materials and Atoms* 268.11-12 (2010), pp. 1703–1710. DOI: 10.1016/j.nimb.2010.02.011 (cit. on p. 6).

[26] A. Jesus et al. "Influence of target thickness on resonant elastic scattering of protons by 19F". In: *Nuclear Instruments and Methods in Physics Research Section B: Beam Interactions with Materials and Atoms* 174.3 (2001), pp. 229–234. DOI: 10.1016/S0168-583X(00)00521-8 (cit. on p. 6).

[27] G. Dearnaley. "LXXXIV. The elastic scattering of protons by light elements". In: *Philosophical Magazine* 1.9 (1956), pp. 821–834. DOI: 10.1080/14786435608238159 (cit. on p. 6).

[28] J. Knox and J. Harmon. “Non-Rutherford elastic scattering in fluorine”. In: *Nuclear Instruments and Methods in Physics Research Section B: Beam Interactions with Materials and Atoms* 44.1 (1989), pp. 40–42. DOI: `10.1016/0168-583X(89)90686-1` (cit. on p. 6).

[29] T. Webb et al. “Elastic Scattering of Protons by F19”. In: *Physical Review* 99.1 (1955), p. 138. DOI: `10.1103/PhysRev.99.138` (cit. on p. 6).

[30] S. Ouichaoui et al. “States in 20Ne from 19Fe(p, p) and 19Fe(p, α) reactions at Esub(p)=(1.5-2.1) MeV”. In: *Nuovo Cimento. A* 86.2 (1985), pp. 170–182 (cit. on p. 6).

[31] U. Fasoli et al. “The elastic scattering of protons by 6Li in the energy range (1.3÷5.6) MeV”. In: *Il Nuovo Cimento (1955-1965)* 34.6 (1964), pp. 1832–1836. DOI: `10.1007/BF02750584` (cit. on pp. 6, 37).

[32] J. Cruz. “Experimental Study of Proton Induced Nuclear Reactions in 6,7Li”. Faculdade de Ciências e Tecnologias da Universidade NOVA de Lisboa, 2006 (cit. on pp. 6, 13, 17, 37).

[33] P. R. Malmberg. “Elastic Scattering of Protons from Li 7”. In: *Physical Review* 101.1 (1956), p. 114. DOI: `10.1103/PhysRev.101.114` (cit. on pp. 6, 37).

[34] M. Mayer. “Improved physics in SIMNRA 7”. In: *Nuclear Instruments and Methods in Physics Research Section B: Beam Interactions with Materials and Atoms* 332 (2014), pp. 176–180. DOI: `10.1016/j.nimb.2014.02.056` (cit. on pp. 7, 21).

[35] J. L’ecuyer, J. Davies, and N. Matsunami. “How accurate are absolute Rutherford backscattering yields”. In: *Nuclear Instruments and Methods* 160.2 (1979), pp. 337–346. DOI: `10.1016/0029-554X(79)90612-8` (cit. on p. 11).

[36] K. S. Krane. *Introductory Nuclear Physics*. John Wiley & Sons, 1988 (cit. on p. 11).

[37] N. Catarino. *Van de Graaff: Manual de Operação*. URL: `http://www.se.ctn.tecnico.ulisboa.pt/FisNuclear/LATR/Manuais/Manual_VG.pdf` (cit. on p. 12).

[38] M. Mayer. “Ion beam analysis of rough thin films”. In: *Nuclear Instruments and Methods in Physics Research Section B: Beam Interactions with Materials and Atoms* 194.2 (2002), pp. 177–186. DOI: `10.1016/S0168-583X(02)00689-4` (cit. on p. 14).

[39] M. Morháč. “An algorithm for determination of peak regions and baseline elimination in spectroscopic data”. In: *Nuclear Instruments and Methods in Physics Research Section A: Accelerators, Spectrometers, Detectors and Associated Equipment* 600 (2 2009-03), pp. 478–487. ISSN: 01689002. DOI: `10.1016/j.nima.2008.11.132`. URL: `https://linkinghub.elsevier.com/retrieve/pii/S0168900208017956` (cit. on p. 14).

[40] C. Ryan et al. "SNIP, a statistics-sensitive background treatment for the quantitative analysis of PIXE spectra in geoscience applications". In: *Nuclear Instruments and Methods in Physics Research Section B: Beam Interactions with Materials and Atoms* 34 (3 1988-09), pp. 396–402. ISSN: 0168583X. DOI: 10.1016/0168-583X(88)90063-8. URL: https://linkinghub.elsevier.com/retrieve/pii/0168583X88900638 (cit. on pp. 14, 15).

[41] M. Morháč et al. "Background elimination methods for multidimensional coincidence γ-ray spectra". In: *Nuclear Instruments and Methods in Physics Research Section A: Accelerators, Spectrometers, Detectors and Associated Equipment* 401 (1 1997-12), pp. 113–132. ISSN: 01689002. DOI: 10.1016/S0168-9002(97)01023-1. URL: https://linkinghub.elsevier.com/retrieve/pii/S0168900297010231 (cit. on p. 15).

[42] M. Morháč and V. Matoušek. "Peak Clipping Algorithms for Background Estimation in Spectroscopic Data". In: *Applied Spectroscopy, Vol. 62, Issue 1, pp. 91-106* 62 (1 2008-01), pp. 91–106. URL: https://opg.optica.org/as/abstract.cfm?uri=as-62-1-91 (cit. on p. 15).

[43] R. Shi et al. "Step-approximation SNIP background-elimination algorithm for HPGe gamma spectra". In: *Nuclear Instruments and Methods in Physics Research Section A: Accelerators, Spectrometers, Detectors and Associated Equipment* 885 (2018-03), pp. 60–66. ISSN: 01689002. DOI: 10.1016/j.nima.2017.12.064. URL: https://linkinghub.elsevier.com/retrieve/pii/S0168900217314705 (cit. on pp. 16, 29).

[44] D. Erb. *pybaselines: A Python library of algorithms for the baseline correction of experimental data*. Version 1.0.0. DOI: 10.5281/zenodo.5608581. URL: https://github.com/derb12/pybaselines (cit. on p. 17).

[45] C. E. Rolfs and W. S. Rodney. *Cauldrons in the cosmos: Nuclear astrophysics*. University of Chicago press, 1988 (cit. on p. 24).

[46] V. Paneta et al. "Differential cross-section measurements for the 7Li(p, p0)7Li, 7Li(p, p1)7Li, 7Li(p, α0)4He, 19F(p, p0)19F, 19F(p, α0)16O and 19F(p, α1, 2)16O reactions". In: *Nuclear Instruments and Methods in Physics Research Section B: Beam Interactions with Materials and Atoms* 288 (2012), pp. 53–59. DOI: 10.1016/j.nimb.2012.07.020 (cit. on pp. 36, 39).

A

Tables of Elemental Depth Profiles

Table A.1: ^{6}Li Target Composition

Layer	Thickness (10^{15} at./cm^2)	^{6}Li (%)	C (%)	O (%)	H (%)	Al (%)
1	300	4.446	16.534	26.742	8.972	43.306
2	300	6.114	8.854	14.609	8.961	61.463
3	200	9.262	4.989	10.603	5.607	69.539
4	200	7.931	4.665	8.935	4.227	74.243
5	200	4.806	2.963	7.921	4.468	79.842
6	200	2.968	2.568	8.545	3.084	82.834
7	200	1.713	2.065	6.196	2.708	87.318
8	200	1.274	1.797	6.530	2.519	87.880
9	200	0.607	2.129	4.959	2.393	89.913
10	200	0.906	2.111	4.232	2.060	90.691
11	200	0.803	1.365	3.496	2.434	91.902
12	Substrate	0	0	0	0	100

Table A.2: ^{7}Li Target Composition

Layer	Thickness (10^{15} at./cm^2)	^{6}Li (%)	C (%)	O (%)	H (%)	Al (%)
1	372.585	13.440	40.000	20.000	11.000	15.560
2	273.307	9.771	26.714	35.000	11.000	17.515
3	178.337	7.811	22.189	30.000	11.000	29.000
4	224.061	6.413	17.575	27.000	11.000	38.012
5	224.413	4.538	13.915	23.623	11.000	46.924
6	202.856	5.048	11.267	22.657	11.000	50.028
7	212.637	5.864	9.030	21.645	11.000	52.462
8	207.782	5.071	7.274	20.655	9.000	58.000
9	206.396	4.459	5.868	19.672	11.000	59.000

10	200.792	4.022	4.762	18.716	11.000	61.500
11	223.188	3.594	3.775	17.653	11.000	63.978
12	205.410	2.277	3.048	16.675	11.000	67.000
13	244.343	2.139	2.364	15.511	11.000	68.986
14	231.436	0	1.858	14.409	11.000	72.733
15	195.868	0	1.516	13.476	11.000	74.008
16	221.496	0	1.204	12.422	11.000	75.375
17	197.537	0	0.980	11.481	11.000	76.539
18	219.328	0	0.780	10.436	11.000	77.784
19	202.505	0	0.632	9.472	11.000	78.896
20	199.397	0	0.513	8.522	11.000	79.964
21	200.000	0	0.417	7.570	11.000	81.013
22	199.974	0	0.339	6.618	11.000	82.044
23	200.000	0	0.275	5.665	11.000	83.060
24	197.744	0	0.224	4.723	11.000	84.053
25	200.000	0	0.182	3.771	11.000	85.047
26	200.000	0	0.148	2.819	11.000	86.034
27	199.964	0	0.120	1.866	11.000	87.014
28	195.278	0	0.098	0.936	11.000	87.966
29	208.767	0	0.079	0.000	11.000	88.921
30	201.586	0	0	0	9.000	91.000
31	Substrate	0	0	0	0	100

B

PROPAGATION OF UNCERTAINTY FORMULAE

$$u(\sigma(\theta)) = \sqrt{u(Y)^2(\frac{e}{N\Omega Q})^2 + u(N)^2(\frac{Ye}{N^2\Omega Q})^2 + u(\Omega)^2(\frac{Ye}{N\Omega^2 Q})^2 + u(Q)^2(\frac{Ye}{N\Omega Q^2})^2}$$

$$\begin{aligned} u(\sigma_R(\theta)) = \Bigg(& \left(\frac{Z_1^2 Z_2^2 e^4}{2E} \frac{1}{\sin^4\theta} \frac{\left(\cos\theta + \sqrt{1-(M_1/M_2)^2\sin^2\theta}\right)^2}{\sqrt{1-(M_1/M_2)^2\sin^2\theta}} \right)^2 u(E)^2 + \\ & \left(\left(\frac{Z_1 Z_2 e^2}{4E} \right)^2 \frac{4}{\sin^4\theta} \frac{\cos\theta + \sqrt{1-(M_1/M_2)^2\sin^2\theta}}{\sqrt{1-(M_1/M_2)^2\sin^2\theta}} \left(-\frac{4}{\tan\theta} \left(\cos\theta + \sqrt{1-(M_1/M_2)^2\sin^2\theta}\right) + \right.\right. \\ & \left.\left. \frac{\sin(2\theta)(M_1/M_2)^2 \left(\cos\theta + \sqrt{1-(M_1/M_2)^2\sin^2\theta}\right)}{1-(M_1/M_2)^2\sin^2\theta} - 2\sin\theta - \frac{2\sin(2\theta)(M_1/M_2)^2}{\sqrt{1-(M_1/M_2)^2\sin^2\theta}} \right) \right)^2 u(\theta)^2 \Bigg)^{1/2} \end{aligned}$$

$$u(\sigma_{R_{cor}}(\theta)) = \sqrt{\left(1 - \frac{0.049 Z_1 Z_2^{4/3}}{E_{CM}}\right)^2 u(\sigma_R(\theta))^2 + \left(\frac{0.049 Z_1 Z_2^{4/3}}{E_{CM}^2}\sigma_R(\theta)\right)^2 u(E_{CM})^2}$$

$$u(n) = \sqrt{\left(\frac{1}{Y_{Ag}}\frac{\sigma_{R_{Ag}}}{\sigma_{R_F}}\right)^2 u(Y_F)^2 + \left(\frac{Y_F}{Y_{Ag}^2}\frac{\sigma_{R_{Ag}}}{\sigma_{R_F}}\right)^2 u(Y_{Ag})^2 + \left(\frac{Y_F}{Y_{Ag}}\frac{\sigma_{R_{Ag}}}{\sigma_{R_F}^2}\right)^2 u(\sigma_{R_F})^2 + \left(\frac{Y_F}{Y_{Ag}}\frac{1}{\sigma_{R_F}}\right)^2 u(\sigma_{R_{Ag}})^2}$$

$$\begin{aligned} u(\sigma(\theta)) = \Bigg(& \left(\frac{\sigma_{R_{Ag}}}{n \times Y_{Ag} \times \sigma_{R_F}}\right)^2 u(Y_F)^2 + \left(\frac{Y_F \times \sigma_{R_{Ag}}}{n \times Y_{Ag}^2 \times \sigma_{R_F}}\right)^2 u(Y_{Ag})^2 + \left(\frac{Y_F \times \sigma_{R_{Ag}}}{n^2 \times Y_{Ag} \times \sigma_{R_F}}\right)^2 u(n)^2 + \\ & \left(\frac{Y_F \times \sigma_{R_{Ag}}}{n \times Y_{Ag} \times \sigma_{R_F}^2}\right)^2 u(\sigma_{R_F})^2 + \left(\frac{Y_F}{n \times Y_{Ag} \times \sigma_{R_F}}\right)^2 u(\sigma_{R_{Ag}})^2 \Bigg)^{1/2} \end{aligned}$$

C

CROSS SECTION TABLES

Table C.1: ^{3}He induced nuclear reactions in ^{7}Li for θ_{lab} = 115°

		^{7}Li(^{3}He, p_0)^{9}Be			^{7}Li(^{3}He, p_2)^{9}Be			^{7}Li(^{3}He, $p_{3,4}$)^{9}Be			^{7}Li(^{3}He, d_0)^{8}Be		
			Uncertainty			Uncertainty			Uncertainty			Uncertainty	
E (keV)	Uncertainty	dσ/dΩ (mb/sr)	Statist.	Total	dσ/dΩ (mb/sr)	Statist.	Total	dσ/dΩ (mb/sr)	Statist.	Total	dσ/dΩ (mb/sr)	Statist.	Total
2375.1	11	0.97	0.108	0.112	1.55	0.174	0.180	0.31	0.088	0.089	1.18	0.130	0.135
2278.4	11	0.93	0.105	0.109	2.12	0.232	0.241	0.30	0.082	0.083	1.23	0.136	0.141
2181.4	10	0.94	0.104	0.108	2.38	0.259	0.269	0.32	0.087	0.087	1.18	0.129	0.134
2083.8	10	0.80	0.089	0.092	2.49	0.268	0.278	0.33	0.089	0.090	0.95	0.106	0.110
1983.9	10	0.63	0.072	0.075	2.06	0.222	0.231	0.28	0.074	0.075	0.82	0.092	0.096
1890.1	9	0.65	0.079	0.081	1.69	0.257	0.262	0.22	0.085	0.085	0.72	0.088	0.091
1789.9	9	0.64	0.071	0.074	1.42	0.155	0.161	0.23	0.052	0.052	0.61	0.069	0.071
1691.7	9	0.62	0.069	0.071	1.24	0.136	0.141	0.24	0.060	0.061	0.47	0.053	0.055
1592.1	8	0.60	0.066	0.069	1.07	0.119	0.123	0.25	0.054	0.054	0.36	0.042	0.044
1493.2	8	0.62	0.069	0.072	1.09	0.121	0.125	0.26	0.056	0.057	0.33	0.038	0.040
1394.3	8	0.76	0.083	0.086	1.11	0.122	0.127	0.27	0.050	0.051	0.32	0.038	0.039
1295.7	8	0.74	0.082	0.085	1.14	0.125	0.129	0.26	0.068	0.069	0.28	0.034	0.035
1197.6	7	0.65	0.072	0.075	1.05	0.117	0.121	0.26	0.063	0.064	0.27	0.033	0.034
1101.9	7	0.60	0.067	0.069	0.99	0.110	0.114	0.38	0.074	0.074	0.20	0.025	0.026
1006.1	7	0.42	0.048	0.050	0.75	0.085	0.088	0.41	0.091	0.091	0.13	0.018	0.018
908.5	7	0.28	0.033	0.034	0.57	0.066	0.068	0.34	0.064	0.065	0.07	0.011	0.011
811.0	6	0.18	0.023	0.024	0.35	0.043	0.044	0.28	0.054	0.054	0.04	0.008	0.008
725.2	6	0.08	0.012	0.012	0.15	0.021	0.022	0.14	0.027	0.027	0.02	0.005	0.005

Table C.2: ^{3}He induced nuclear reactions in ^{7}Li for θ_{lab} = 125°

		^{7}Li(^{3}He, p_0)^{9}Be			^{7}Li(^{3}He, p_2)^{9}Be			^{7}Li(^{3}He, $p_{3,4}$)^{9}Be			^{7}Li(^{3}He, d_0)^{8}Be		
			Uncertainty			Uncertainty			Uncertainty			Uncertainty	
E (keV)	Uncertainty	dσ/dΩ (mb/sr)	Statist.	Total	dσ/dΩ (mb/sr)	Statist.	Total	dσ/dΩ (mb/sr)	Statist.	Total	dσ/dΩ (mb/sr)	Statist.	Total
2374.8	11	0.77	0.087	0.090	1.63	0.181	0.187	0.23	0.068	0.068	1.20	0.134	0.138
2279.1	11	0.76	0.087	0.090	1.88	0.210	0.217	0.28	0.090	0.091	1.15	0.130	0.135
2180.6	10	0.79	0.089	0.092	2.21	0.240	0.249	0.31	0.089	0.089	1.10	0.122	0.126
2082.5	10	0.64	0.072	0.074	2.37	0.255	0.264	0.24	0.073	0.074	0.99	0.110	0.114
1986.1	10	0.63	0.070	0.072	2.12	0.228	0.236	0.20	0.051	0.051	0.90	0.098	0.102

1887.9	9	0.51	0.058	0.060	1.64	0.177	0.183	0.21	0.056	0.057	0.68	0.077	0.079
1789.6	9	0.51	0.058	0.060	1.39	0.152	0.158	0.22	0.073	0.073	0.55	0.063	0.065
1691.1	9	0.48	0.055	0.057	1.14	0.125	0.130	0.23	0.051	0.051	0.49	0.056	0.058
1594.0	8	0.53	0.059	0.061	0.97	0.108	0.112	0.22	0.050	0.050	0.39	0.045	0.047
1493.0	8	0.59	0.066	0.068	1.04	0.114	0.118	0.21	0.047	0.047	0.34	0.039	0.041
1394.6	8	0.67	0.074	0.077	1.03	0.114	0.119	0.22	0.059	0.060	0.32	0.038	0.039
1296.4	8	0.65	0.072	0.075	0.95	0.105	0.109	0.22	0.065	0.066	0.28	0.034	0.035
1199.5	7	0.62	0.070	0.072	1.02	0.112	0.116	0.25	0.057	0.058	0.24	0.029	0.030
1102.2	7	0.54	0.062	0.064	0.83	0.093	0.096	0.28	0.067	0.068	0.16	0.021	0.022
1005.4	7	0.36	0.042	0.043	0.72	0.082	0.084	0.28	0.066	0.066	0.12	0.016	0.017
910.5	7	0.29	0.034	0.035	0.53	0.061	0.063	0.27	0.062	0.062	0.06	0.010	0.010
808.8	6	0.18	0.023	0.023	0.34	0.041	0.042	0.24	0.057	0.058	0.03	0.007	0.007
709.0	6	0.08	0.012	0.012	0.13	0.020	0.021	0.14	0.036	0.037	0.02	0.004	0.004

Table C.3: ^{3}He induced nuclear reactions in ^{7}Li for θ_{lab} = 135^o

		^{7}Li(^{3}He, p_0)^{9}Be			^{7}Li(^{3}He, p_2)^{9}Be			^{7}Li(^{3}He, $p_{3,4}$)^{9}Be			^{7}Li(^{3}He, d_0)^{8}Be		
			Uncertainty			Uncertainty			Uncertainty			Uncertainty	
E (keV)	Uncertainty	dσ/dΩ (mb/sr)	Statist.	Total	dσ/dΩ (mb/sr)	Statist.	Total	dσ/dΩ (mb/sr)	Statist.	Total	dσ/dΩ (mb/sr)	Statist.	Total
2375.5	11	1.11	0.123	0.127	1.19	0.137	0.142	0.29	0.073	0.074	0.85	0.099	0.103
2279.0	11	1.11	0.123	0.128	1.32	0.154	0.159	0.36	0.102	0.103	0.84	0.100	0.103
2182.1	10	1.08	0.118	0.123	1.58	0.176	0.182	0.35	0.098	0.098	0.74	0.087	0.090
2084.2	10	1.00	0.110	0.114	1.60	0.178	0.184	0.25	0.073	0.073	0.55	0.068	0.070
1983.9	10	0.86	0.095	0.099	1.43	0.158	0.164	0.22	0.071	0.071	0.48	0.060	0.062
1884.6	9	0.73	0.087	0.089	1.15	0.137	0.141	0.26	0.081	0.082	0.48	0.059	0.061
1791.2	9	0.75	0.083	0.086	0.99	0.111	0.115	0.19	0.066	0.066	0.37	0.043	0.045
1691.1	9	0.76	0.084	0.087	1.00	0.113	0.117	0.22	0.064	0.064	0.31	0.036	0.037
1591.0	8	0.69	0.076	0.078	0.98	0.110	0.114	0.25	0.053	0.054	0.24	0.030	0.031
1491.1	8	0.76	0.083	0.086	0.99	0.109	0.113	0.24	0.059	0.059	0.26	0.031	0.032
1393.4	8	0.84	0.091	0.095	1.09	0.120	0.125	0.24	0.058	0.059	0.29	0.034	0.035
1295.6	8	0.76	0.083	0.086	1.07	0.119	0.123	0.26	0.073	0.074	0.25	0.031	0.032
1197.2	7	0.70	0.078	0.080	0.94	0.105	0.109	0.27	0.064	0.065	0.25	0.031	0.031
1101.9	7	0.62	0.070	0.072	0.88	0.099	0.102	0.32	0.080	0.081	0.19	0.024	0.025
1005.9	7	0.46	0.052	0.054	0.75	0.086	0.088	0.33	0.078	0.078	0.12	0.016	0.017

909.2	7	0.32	0.037	0.038	0.51	0.060	0.062	0.33	0.077	0.077	0.07	0.011	0.011
806.9	6	0.21	0.026	0.026	0.34	0.043	0.044	0.29	0.065	0.065	0.03	0.007	0.007
697.3	6	0.09	0.013	0.013	0.15	0.020	0.020	0.18	0.033	0.033	0.03	0.006	0.006

Table C.4: ^{3}He induced nuclear reactions in ^{7}Li for $\theta_{lab} = 145^o$

		^{7}Li(^{3}He, p$_0$)^{9}Be			^{7}Li(^{3}He, p$_2$)^{9}Be			^{7}Li(^{3}He, p$_{3,4}$)^{9}Be			^{7}Li(^{3}He, d$_0$)^{8}Be		
			Uncertainty			Uncertainty			Uncertainty			Uncertainty	
E (keV)	Uncertainty	dσ/dΩ (mb/sr)	Statist.	Total	dσ/dΩ (mb/sr)	Statist.	Total	dσ/dΩ (mb/sr)	Statist.	Total	dσ/dΩ (mb/sr)	Statist.	Total
2374.9	11	1.05	0.116	0.121	1.31	0.152	0.157	0.36	0.098	0.099	1.10	0.123	0.128
2279.3	11	1.04	0.116	0.120	1.59	0.179	0.185	0.33	0.087	0.088	1.04	0.118	0.122
2181.1	10	1.00	0.110	0.114	2.02	0.220	0.228	0.32	0.082	0.083	0.97	0.109	0.113
2083.3	10	0.94	0.103	0.107	1.89	0.206	0.213	0.28	0.061	0.062	0.81	0.091	0.094
1986.3	10	0.82	0.090	0.093	1.67	0.181	0.188	0.23	0.062	0.063	0.67	0.075	0.078
1886.6	9	0.74	0.081	0.084	1.33	0.145	0.151	0.21	0.056	0.056	0.55	0.062	0.064
1790.1	9	0.70	0.077	0.080	1.12	0.125	0.130	0.22	0.055	0.056	0.52	0.058	0.060
1692.7	9	0.67	0.074	0.077	1.04	0.116	0.120	0.20	0.059	0.060	0.35	0.042	0.043
1591.2	8	0.66	0.073	0.076	0.99	0.110	0.114	0.21	0.058	0.058	0.29	0.034	0.035
1491.8	8	0.70	0.078	0.080	1.02	0.113	0.117	0.20	0.059	0.059	0.30	0.035	0.037
1394.0	8	0.83	0.091	0.095	1.10	0.121	0.125	0.24	0.056	0.057	0.31	0.036	0.037
1296.8	8	0.72	0.079	0.082	1.10	0.121	0.125	0.25	0.068	0.069	0.27	0.032	0.033
1197.7	7	0.72	0.080	0.083	1.06	0.118	0.122	0.25	0.070	0.071	0.22	0.028	0.028
1100.5	7	0.58	0.066	0.068	1.00	0.111	0.115	0.26	0.065	0.065	0.20	0.025	0.025
1006.5	7	0.45	0.052	0.054	0.77	0.087	0.090	0.29	0.068	0.068	0.13	0.018	0.018
911.3	7	0.33	0.039	0.040	0.58	0.067	0.069	0.34	0.055	0.056	0.07	0.011	0.011
817.5	6	0.18	0.023	0.023	0.31	0.039	0.040	0.23	0.052	0.053	0.03	0.007	0.007
729.0	6	0.08	0.012	0.012	0.16	0.023	0.023	0.12	0.035	0.035	0.01	0.004	0.004

Table C.5: ^{3}He induced nuclear reactions in ^{7}Li for $\theta_{lab} = 155^o$

		^{7}Li(^{3}He, p$_0$)^{9}Be			^{7}Li(^{3}He, p$_2$)^{9}Be			^{7}Li(^{3}He, d$_0$)^{8}Be		
			Uncertainty			Uncertainty			Uncertainty	
E (keV)	Uncertainty	dσ/dΩ (mb/sr)	Statist.	Total	dσ/dΩ (mb/sr)	Statist.	Total	dσ/dΩ (mb/sr)	Statist.	Total
2375.6	11	1.13	0.124	0.129	0.89	0.120	0.123	0.48	0.065	0.067

2279.1	11	1.17	0.130	0.135	0.88	0.117	0.120	0.47	0.062	0.064
2181.4	10	1.21	0.132	0.136	0.97	0.127	0.130	0.40	0.054	0.055
2083.4	10	1.14	0.125	0.129	0.93	0.116	0.119	0.37	0.052	0.053
1985.7	10	1.03	0.113	0.117	0.92	0.115	0.118	0.30	0.043	0.044
1877.2	9	1.02	0.116	0.120	0.99	0.132	0.135	0.33	0.044	0.045
1792.5	9	0.98	0.106	0.110	0.87	0.107	0.111	0.24	0.029	0.030
1692.6	9	0.87	0.095	0.099	0.87	0.108	0.111	0.17	0.026	0.027
1589.0	8	0.86	0.093	0.097	0.90	0.109	0.112	0.12	0.021	0.021
1488.4	8	0.74	0.081	0.084	0.95	0.112	0.115	0.19	0.024	0.024
1391.2	8	0.87	0.095	0.098	1.01	0.120	0.124	0.23	0.028	0.029
1294.1	8	0.81	0.088	0.091	0.99	0.119	0.122	0.25	0.030	0.031
1197.6	7	0.72	0.079	0.082	0.93	0.111	0.114	0.24	0.029	0.030
1102.1	7	0.63	0.070	0.073	0.79	0.101	0.103	0.18	0.023	0.024
1004.5	7	0.49	0.056	0.057	0.65	0.082	0.084	0.11	0.015	0.016
906.0	7	0.35	0.040	0.042	0.49	0.062	0.064	0.08	0.012	0.012
808.0	6	0.19	0.023	0.024	0.28	0.042	0.043	0.04	0.007	0.007
704.5	6	0.08	0.012	0.012	0.14	0.021	0.021	0.03	0.005	0.005

Table C.6: ^{3}He induced nuclear reactions in ^{7}Li for $\theta_{lab} = 165^o$

		^{7}Li(^{3}He, p_0)^{9}Be			^{7}Li(^{3}He, p_2)^{9}Be			^{7}Li(^{3}He, $p_{3,4}$)^{9}Be			^{7}Li(^{3}He, d_0)^{8}Be		
			Uncertainty			Uncertainty			Uncertainty			Uncertainty	
E (keV)	Uncertainty	dσ/dΩ (mb/sr)	Statist.	Total	dσ/dΩ (mb/sr)	Statist.	Total	dσ/dΩ (mb/sr)	Statist.	Total	dσ/dΩ (mb/sr)	Statist.	Total
2374.4	11	1.23	0.135	0.140	1.07	0.131	0.135	-	-	-	0.62	0.085	0.087
2280.1	11	1.16	0.128	0.132	1.09	0.132	0.136	0.32	0.104	0.105	0.62	0.076	0.079
2181.8	10	1.20	0.131	0.136	1.18	0.145	0.149	0.30	0.097	0.098	0.44	0.054	0.056
2082.5	10	1.05	0.122	0.126	1.17	0.141	0.146	0.30	0.077	0.077	0.43	0.056	0.058
1986.0	10	1.07	0.116	0.120	1.06	0.123	0.128	0.28	0.081	0.081	0.36	0.047	0.048
1886.4	9	0.86	0.099	0.102	1.00	0.118	0.122	0.25	0.079	0.080	0.31	0.039	0.040
1789.8	9	0.83	0.090	0.094	0.91	0.108	0.111	0.22	0.056	0.056	0.29	0.038	0.039
1689.8	9	0.81	0.088	0.091	0.92	0.110	0.113	0.18	0.052	0.052	0.21	0.029	0.030
1595.2	8	0.88	0.096	0.099	0.90	0.105	0.109	0.16	0.043	0.044	0.20	0.024	0.025
1490.7	8	0.74	0.082	0.084	1.01	0.117	0.121	0.15	0.048	0.048	0.21	0.025	0.026
1393.0	8	0.84	0.092	0.095	1.05	0.123	0.127	0.16	0.043	0.043	0.25	0.030	0.031

1293.9	8	0.73	0.080	0.083	0.99	0.117	0.121	0.20	0.055	0.055	0.22	0.027	0.028
1196.4	7	0.74	0.082	0.085	0.93	0.110	0.114	0.24	0.079	0.079	0.26	0.031	0.032
1102.1	7	0.65	0.072	0.075	0.85	0.101	0.104	0.24	0.067	0.067	0.19	0.024	0.024
1005.8	7	0.46	0.053	0.054	0.65	0.081	0.083	0.23	0.049	0.049	0.13	0.017	0.018
909.2	7	0.36	0.041	0.042	0.49	0.062	0.063	0.20	0.054	0.055	0.07	0.011	0.011
816.7	6	0.21	0.026	0.027	0.32	0.045	0.046	0.18	0.054	0.055	0.04	0.007	0.008
731.9	6	0.07	0.011	0.011	0.13	0.022	0.022	0.14	0.040	0.041	0.01	0.004	0.004

Table C.7: ^{6}Li(^{3}He, p_0)^{8}Be for θ_{lab} = 115°, 135°, 155°

		115°			135°			155°		
			Uncertainty			Uncertainty			Uncertainty	
E (keV)	Uncertainty	dσ/dΩ (mb/sr)	Statist.	Total	dσ/dΩ (mb/sr)	Statist.	Total	dσ/dΩ (mb/sr)	Statist.	Total
2382.3	11	1.37	0.157	0.162	1.03	0.121	0.125	0.43	0.057	0.058
2286.0	11	1.39	0.159	0.164	0.91	0.108	0.111	0.47	0.060	0.062
2188.8	10	1.22	0.139	0.144	0.96	0.112	0.115	0.54	0.067	0.069
2090.5	10	1.11	0.128	0.132	0.88	0.104	0.107	0.55	0.068	0.070
1992.8	10	1.16	0.136	0.140	0.85	0.103	0.106	0.56	0.071	0.073
1893.3	9	1.14	0.141	0.145	0.90	0.115	0.118	0.65	0.087	0.089
1797.0	9	1.08	0.120	0.125	0.94	0.105	0.109	0.58	0.068	0.070
1698.1	9	1.26	0.140	0.145	0.89	0.100	0.104	0.58	0.068	0.070
1648.9	9	1.19	0.132	0.137	0.97	0.108	0.112	0.61	0.070	0.073
1600.5	8	1.21	0.135	0.140	1.01	0.113	0.117	0.68	0.078	0.081
1502.9	8	1.17	0.130	0.135	0.90	0.101	0.105	0.68	0.078	0.081
1404.9	8	1.03	0.116	0.120	0.77	0.088	0.091	0.59	0.069	0.071
1306.0	8	0.91	0.103	0.107	0.80	0.091	0.094	0.54	0.064	0.066
1205.8	7	0.94	0.107	0.111	0.72	0.084	0.086	0.52	0.061	0.063
1107.8	7	0.98	0.111	0.115	0.76	0.087	0.090	0.53	0.063	0.065
1009.1	7	0.86	0.099	0.103	0.68	0.080	0.082	0.48	0.058	0.060
1008.6	7	1.01	0.126	0.129	0.73	0.095	0.097	0.36	0.054	0.055
917.6	7	0.49	0.058	0.060	0.40	0.048	0.050	0.32	0.039	0.040
816.0	6	0.30	0.038	0.040	0.30	0.038	0.039	0.31	0.039	0.040
718.0	6	0.20	0.028	0.029	0.20	0.028	0.028	0.19	0.026	0.027

Table C.8: $^{6}\text{Li}(^{3}\text{He}, p_{0})^{8}\text{Be}$ for θ_{lab} = 125°, 145°, 165°

		125°			145°			165°		
			Uncertainty			Uncertainty			Uncertainty	
E (keV)	Uncertainty	dσ/dΩ (mb/sr)	Statist.	Total	dσ/dΩ (mb/sr)	Statist.	Total	dσ/dΩ (mb/sr)	Statist.	Total
2383.0	11	1.43	0.162	0.168	1.03	0.120	0.124	0.68	0.082	0.085
2286.0	11	1.19	0.138	0.143	1.08	0.125	0.129	0.66	0.081	0.083
2189.0	10	1.16	0.133	0.138	1.03	0.118	0.122	0.69	0.082	0.085
2089.6	10	1.22	0.137	0.142	0.99	0.112	0.116	0.68	0.079	0.081
1993.0	10	1.09	0.124	0.128	1.07	0.121	0.125	0.71	0.083	0.086
1894.1	9	1.08	0.120	0.124	1.07	0.119	0.123	0.74	0.084	0.087
1797.1	9	1.09	0.122	0.126	0.93	0.105	0.109	0.70	0.081	0.083
1698.0	9	1.11	0.124	0.128	0.98	0.110	0.114	0.73	0.084	0.086
1649.4	9	1.15	0.128	0.133	1.12	0.124	0.129	0.80	0.090	0.093
1600.1	9	1.07	0.120	0.124	1.00	0.112	0.116	0.74	0.084	0.087
1503.0	9	1.14	0.127	0.132	1.14	0.126	0.131	0.66	0.077	0.079
1405.1	9	0.93	0.106	0.110	0.76	0.087	0.090	0.71	0.082	0.084
1306.0	8	0.83	0.095	0.099	0.83	0.095	0.098	0.57	0.067	0.069
1206.1	8	0.86	0.099	0.102	0.78	0.090	0.093	0.62	0.073	0.075
1108.1	8	0.89	0.102	0.105	0.82	0.094	0.097	0.64	0.074	0.077
1011.4	8	0.79	0.092	0.095	0.70	0.082	0.084	0.57	0.067	0.069
914.6	7	0.55	0.065	0.067	0.51	0.061	0.063	0.46	0.056	0.057
816.6	7	0.33	0.043	0.045	0.41	0.051	0.053	0.37	0.047	0.048
719.0	7	0.21	0.030	0.031	0.19	0.028	0.029	0.17	0.026	0.026

Table C.9: (p,p) reactions for θ_{lab} = 165°

		$^{19}\text{F}(p, p)^{19}\text{F}$			$^{7}\text{Li}(p, p)^{7}\text{Li}$			$^{6}\text{Li}(p, p)^{6}\text{Li}$		
			Uncertainty			Uncertainty			Uncertainty	
E (keV)	Uncertainty	dσ/dΩ (rr)	Statist.	Total	dσ/dΩ (rr)	Statist.	Total	dσ/dΩ (mb/sr)	Statist.	Total
2038.6	8	1.05	0.06	0.07	37.7	1.9	2.0	111.4	26.7	26.7
2038.6	8	0.98	0.04	0.05	37.9	1.8	1.8	77.4	10.1	10.1
2012.0	8	0.79	0.05	0.06	35.2	1.8	1.9	101.7	26.5	26.5
1989.3	7	0.84	0.06	0.06	30.8	1.6	1.7	122.1	26.3	26.3
1969.6	7	0.99	0.06	0.07	26.8	1.5	1.5	95.3	21.1	21.1

1959.8	7	1.05	0.06	0.07	24.8	1.4	1.4	115.9	26.6	26.6
1953.8	7	1.04	0.10	0.10	23.0	1.3	1.4	76.9	20.0	20.0
1949.9	7	1.02	0.06	0.06	21.7	1.3	1.3	107.2	27.2	27.2
1946.0	7	0.96	0.06	0.07	20.6	1.2	1.3	123.1	31.8	31.8
1942.0	7	0.90	0.06	0.06	19.7	1.2	1.2	116.9	27.2	27.2
1938.1	7	0.83	0.06	0.07	18.6	1.1	1.2	117.6	29.0	29.0
1934.1	7	0.64	0.06	0.06	17.6	1.2	1.2	106.7	23.7	23.7
1930.2	7	0.50	0.09	0.09	17.0	1.1	1.2	105.7	25.2	25.2
1926.2	7	0.41	0.05	0.05	15.6	1.2	1.2	84.2	22.9	22.9
1920.3	7	0.37	0.05	0.06	13.9	1.2	1.2	91.9	24.7	24.7
1916.4	7	0.56	0.05	0.06	12.1	0.8	0.9	101.0	23.7	23.7
1910.4	7	0.83	0.07	0.07	11.3	0.8	0.8	115.5	24.2	24.2
1905.5	7	1.21	0.07	0.08	10.5	0.8	0.8	117.9	30.0	30.0
1900.6	7	1.29	0.07	0.08	9.7	0.7	0.7	107.2	22.6	22.6
1895.6	7	1.20	0.07	0.08	9.1	0.8	0.8	96.7	24.2	24.2
1890.7	7	1.17	0.07	0.08	8.0	0.7	0.7	103.1	20.3	20.3
1885.8	7	1.19	0.07	0.08	7.6	0.8	0.8	124.0	28.9	28.9
1880.8	7	1.14	0.13	0.13	8.3	0.8	0.8	107.3	21.9	21.9
1871.0	7	1.11	0.06	0.07	7.4	0.8	0.8	118.3	27.4	27.4
1851.2	7	1.19	0.07	0.08	8.4	0.8	0.8	146.0	34.3	34.3
1831.5	7	1.38	0.07	0.08	7.7	0.7	0.7	132.4	26.6	26.6
1811.7	7	1.46	0.09	0.09	7.4	0.7	0.7	124.5	23.9	23.9
1792.0	7	1.47	0.10	0.10	6.2	0.6	0.6	145.5	29.1	29.1
1772.2	7	1.59	0.08	0.09	6.4	0.6	0.6	155.3	26.6	26.6
1767.3	7	1.66	0.08	0.09	6.4	0.6	0.6	148.8	23.0	23.0
1762.3	7	1.69	0.08	0.09	6.3	0.6	0.6	113.0	20.2	20.2
1754.4	7	1.68	0.08	0.10	6.3	0.6	0.6	144.4	30.0	30.0
1746.5	7	1.69	0.08	0.10	6.1	0.6	0.6	149.5	28.2	28.2
1738.6	7	1.64	0.10	0.10	6.3	0.6	0.6	145.6	26.1	26.1
1730.7	7	1.59	0.08	0.09	6.3	0.6	0.6	147.2	24.7	24.7
1722.8	7	1.59	0.08	0.09	7.0	0.7	0.7	122.1	18.8	18.8
1703.0	7	1.43	0.08	0.09	5.5	0.5	0.5	138.6	24.6	24.6
1683.3	7	1.04	0.06	0.07	5.9	0.6	0.6	113.2	24.3	24.3

1678.3	7	1.11	0.07	0.07	5.9	0.5	0.5	138.7	26.4	26.4
1673.4	7	1.14	0.06	0.07	6.0	0.6	0.6	135.4	25.9	25.9
1663.5	7	1.13	0.06	0.07	6.2	0.7	0.7	126.3	24.8	24.8
1653.6	6	1.18	0.07	0.08	6.2	0.6	0.6	136.9	25.0	25.0
1633.8	6	1.28	0.06	0.07	6.6	0.5	0.6	113.5	22.3	22.3
1614.0	6	1.37	0.07	0.08	6.2	0.7	0.7	128.8	27.3	27.3
1594.2	6	1.33	0.07	0.08	6.2	0.5	0.5	105.1	22.6	22.6
1574.4	6	1.42	0.07	0.08	6.2	0.5	0.5	116.0	24.4	24.4
1554.6	6	1.51	0.08	0.08	6.4	0.6	0.6	115.2	23.4	23.4
1534.8	6	1.53	0.08	0.09	6.1	0.5	0.5	119.1	27.4	27.4
1515.0	6	1.62	0.08	0.09	5.7	0.6	0.6	99.8	27.6	27.6
1495.1	6	1.64	0.08	0.09	5.7	0.5	0.5	89.7	22.4	22.4
1495.1	6	1.72	0.08	0.09	6.2	0.5	0.5	95.5	28.5	28.5
1480.3	6	1.68	0.08	0.09	5.8	0.5	0.5	109.0	26.0	26.0
1455.5	6	1.98	0.09	0.11	5.5	0.5	0.5	93.5	24.7	24.7
1447.5	6	2.17	0.10	0.12	6.0	0.5	0.5	79.5	24.6	24.6
1441.6	6	2.34	0.10	0.12	5.8	0.5	0.5	77.7	23.1	23.1
1433.7	6	2.79	0.12	0.15	5.7	0.5	0.5	75.7	20.3	20.3
1429.7	6	2.68	0.12	0.14	5.5	0.4	0.4	76.0	21.9	21.9
1427.7	6	2.16	0.10	0.11	5.7	0.5	0.5	65.1	24.8	24.8
1425.7	6	1.76	0.13	0.13	5.7	0.5	0.5	69.0	17.2	17.2
1423.7	6	1.05	0.05	0.06	5.6	0.5	0.5	83.1	22.7	22.7
1421.7	6	0.72	0.11	0.11	5.6	0.5	0.5	85.5	26.3	26.3
1419.8	6	0.56	0.04	0.04	5.2	0.4	0.4	64.4	22.5	22.5
1417.8	6	0.60	0.04	0.04	5.5	0.5	0.5	95.5	26.7	26.7
1415.8	6	0.59	0.05	0.05	5.6	0.4	0.4	53.9	16.6	16.6
1413.8	6	0.60	0.09	0.09	6.1	0.5	0.5	87.9	21.8	21.8
1411.8	6	0.58	0.04	0.04	5.8	0.5	0.5	74.2	25.0	25.0
1409.8	6	0.62	0.04	0.05	5.3	0.4	0.4	76.0	23.6	23.6
1407.9	6	0.69	0.04	0.04	5.1	0.4	0.4	60.2	17.4	17.4
1405.9	6	0.73	0.05	0.05	4.8	0.4	0.4	52.6	15.9	15.9
1403.9	6	0.73	0.04	0.05	5.3	0.4	0.4	65.4	23.6	23.6
1401.9	6	0.77	0.04	0.05	5.1	0.4	0.4	77.1	22.3	22.3

1399.9	6	0.80	0.05	0.05	5.3	0.5	0.5	68.5	19.1	19.1
1397.9	6	0.84	0.10	0.10	5.0	0.4	0.5	65.9	22.0	22.0
1395.9	6	0.83	0.08	0.08	5.2	0.5	0.5	54.1	15.8	15.8
1394.0	6	0.86	0.05	0.06	5.4	0.4	0.4	70.4	21.6	21.6
1392.0	6	0.85	0.04	0.04	5.1	0.3	0.3	60.7	8.7	8.7
1390.0	6	0.87	0.05	0.06	5.4	0.4	0.4	94.5	27.9	27.9
1388.0	6	0.87	0.05	0.05	5.3	0.4	0.5	54.3	20.3	20.3
1386.0	6	0.89	0.05	0.06	5.3	0.4	0.4	65.5	25.0	25.0
1384.0	6	0.80	0.09	0.09	5.0	0.4	0.4	80.7	26.5	26.5
1382.0	6	0.70	0.04	0.05	5.3	0.4	0.4	58.6	20.6	20.6
1380.1	6	0.62	0.04	0.04	5.2	0.5	0.5	59.4	18.6	18.6
1378.1	6	0.50	0.04	0.04	5.0	0.4	0.4	64.9	21.7	21.7
1376.1	6	0.52	0.06	0.06	5.1	0.4	0.4	92.9	26.5	26.5
1374.1	6	0.54	0.04	0.04	5.7	0.5	0.5	65.0	19.2	19.2
1372.1	6	0.66	0.04	0.04	5.5	0.5	0.5	59.8	17.3	17.3
1370.1	6	0.77	0.05	0.05	5.3	0.4	0.4	45.9	15.4	15.4
1368.1	6	0.86	0.05	0.05	5.5	0.5	0.5	56.0	16.9	16.9
1366.2	6	0.97	0.06	0.06	5.2	0.4	0.4	74.7	21.7	21.7
1364.2	6	0.98	0.05	0.06	5.0	0.4	0.4	58.8	22.0	22.0
1362.2	6	1.08	0.07	0.07	5.1	0.4	0.4	45.2	18.8	18.8
1360.2	6	1.05	0.06	0.06	4.9	0.4	0.4	68.1	23.3	23.3
1358.2	6	1.06	0.06	0.07	4.9	0.3	0.3	59.7	21.8	21.8
1356.2	6	1.06	0.05	0.06	5.1	0.4	0.4	-	-	-
1354.2	6	1.04	0.11	0.11	5.0	0.4	0.4	-	-	-
1352.2	6	0.90	0.05	0.05	4.9	0.4	0.4	-	-	-
1349.3	6	0.93	0.05	0.06	5.1	0.4	0.4	-	-	-
1346.3	6	1.03	0.05	0.06	5.1	0.4	0.4	-	-	-
1336.4	6	1.11	0.06	0.06	4.9	0.4	0.4	-	-	-
1316.5	6	1.12	0.06	0.07	4.7	0.4	0.4	-	-	-
1296.6	6	1.18	0.06	0.07	5.1	0.4	0.4	-	-	-
1276.7	6	1.18	0.06	0.07	4.5	0.4	0.4	-	-	-
1256.8	6	1.20	0.06	0.07	4.6	0.4	0.4	-	-	-
1236.9	6	1.16	0.09	0.09	4.5	0.4	0.4	-	-	-

1217.0	6	1.14	0.09	0.09	4.6	0.4	0.4	-	-	-
1197.1	6	1.12	0.06	0.06	4.4	0.4	0.4	-	-	-
1177.2	6	1.11	0.06	0.06	4.8	0.4	0.4	-	-	-
1157.2	6	1.13	0.05	0.06	4.9	0.4	0.4	-	-	-
1137.3	6	1.13	0.06	0.06	4.9	0.4	0.4	-	-	-
1117.3	6	1.09	0.05	0.06	5.0	0.4	0.4	-	-	-
1097.4	6	1.14	0.07	0.07	5.3	0.4	0.4	-	-	-
1077.4	6	1.09	0.05	0.06	5.8	0.4	0.4	-	-	-
1057.4	6	1.09	0.11	0.11	6.0	0.4	0.4	-	-	-
1037.5	6	1.14	0.07	0.07	6.1	0.4	0.4	-	-	-
1017.5	6	1.17	0.06	0.07	5.8	0.4	0.4	-	-	-
997.5	6	1.18	0.06	0.07	5.2	0.4	0.4	-	-	-
987.5	6	1.25	0.10	0.10	4.7	0.4	0.4	-	-	-
977.5	6	1.17	0.06	0.07	3.9	0.3	0.3	-	-	-
967.4	6	1.26	0.06	0.07	3.7	0.3	0.3	-	-	-
957.4	6	1.34	0.10	0.10	3.1	0.3	0.3	-	-	-
953.4	6	1.29	0.11	0.11	3.1	0.3	0.3	-	-	-
949.4	6	1.32	0.07	0.07	2.8	0.3	0.3	-	-	-
945.4	6	1.29	0.06	0.07	2.8	0.3	0.3	-	-	-
941.4	6	1.29	0.09	0.09	2.7	0.3	0.3	-	-	-
937.4	6	1.21	0.07	0.07	2.6	0.2	0.2	-	-	-
933.4	6	1.05	0.05	0.06	2.3	0.2	0.2	-	-	-
929.4	6	1.10	0.05	0.06	2.5	0.3	0.3	-	-	-
925.4	6	1.14	0.07	0.07	2.2	0.2	0.2	-	-	-
921.4	6	1.17	0.06	0.07	2.3	0.2	0.2	-	-	-
917.4	6	1.16	0.06	0.07	2.0	0.2	0.2	-	-	-
907.3	6	1.22	0.06	0.07	1.8	0.2	0.2	-	-	-
897.3	6	1.28	0.06	0.07	1.8	0.2	0.2	-	-	-
887.3	6	1.35	0.08	0.08	1.6	0.2	0.2	-	-	-
883.2	6	1.26	0.06	0.07	1.4	0.2	0.2	-	-	-
879.2	6	1.16	0.08	0.08	1.3	0.2	0.2	-	-	-
875.2	6	0.93	0.06	0.06	1.5	0.2	0.2	-	-	-
871.2	6	1.10	0.05	0.06	1.5	0.2	0.2	-	-	-

867.2	6	1.28	0.06	0.07	1.2	0.2	0.2	-	-	-
863.2	6	1.40	0.07	0.08	1.1	0.2	0.2	-	-	-
859.1	6	1.41	0.07	0.08	1.1	0.1	0.1	-	-	-
855.1	6	1.38	0.07	0.08	1.3	0.2	0.2	-	-	-
851.1	6	1.33	0.06	0.07	1.0	0.2	0.2	-	-	-
847.1	6	1.22	0.06	0.07	1.3	0.2	0.2	-	-	-
847.1	6	1.28	0.07	0.07	1.1	0.2	0.2	-	-	-
843.1	6	1.03	0.05	0.06	1.1	0.2	0.2	-	-	-
839.0	6	0.93	0.05	0.06	0.9	0.2	0.2	-	-	-
835.0	5	0.82	0.04	0.05	1.1	0.2	0.2	-	-	-
831.0	5	0.77	0.05	0.05	1.0	0.2	0.2	-	-	-
827.0	5	0.77	0.04	0.05	1.1	0.3	0.3	-	-	-
823.0	5	0.78	0.04	0.05	0.9	0.2	0.2	-	-	-
818.9	5	0.80	0.05	0.05	0.7	0.2	0.2	-	-	-
814.9	5	0.79	0.05	0.05	0.7	0.2	0.2	-	-	-
810.9	5	0.84	0.05	0.06	0.4	0.1	0.1	-	-	-
806.9	5	0.78	0.09	0.09	0.7	0.2	0.2	-	-	-
802.8	5	0.76	0.10	0.10	0.5	0.2	0.2	-	-	-
798.8	5	0.85	0.05	0.05	0.5	0.1	0.2	-	-	-
786.7	5	0.86	0.08	0.08	0.6	0.2	0.2	-	-	-
766.6	5	0.83	0.05	0.05	0.5	0.2	0.2	-	-	-
746.4	5	0.84	0.05	0.05	0.6	0.2	0.2	-	-	-
736.3	5	0.87	0.05	0.05	0.4	0.2	0.2	-	-	-
726.2	5	0.90	0.05	0.06	0.5	0.2	0.2	-	-	-
716.1	5	0.92	0.09	0.09	0.3	0.1	0.1	-	-	-
711.1	5	0.97	0.15	0.15	0.5	0.1	0.1	-	-	-
706.0	5	0.97	0.08	0.08	0.5	0.2	0.2	-	-	-
701.0	5	1.00	0.06	0.06	0.3	0.1	0.1	-	-	-
695.9	5	0.98	0.06	0.06	0.3	0.1	0.1	-	-	-
690.9	5	1.09	0.06	0.07	0.3	0.1	0.1	-	-	-
685.8	5	1.14	0.06	0.07	0.3	0.1	0.1	-	-	-
680.8	5	1.28	0.16	0.16	0.4	0.1	0.1	-	-	-
675.7	5	1.50	0.17	0.17	0.3	0.1	0.1	-	-	-

670.6	5	1.27	0.10	0.10	0.2	0.1	0.1	-	-	-
665.6	5	0.29	0.03	0.03	0.1	0.1	0.1	-	-	-
660.5	5	0.38	0.30	0.30	0.2	0.1	0.1	-	-	-
655.5	5	0.51	0.25	0.25	0.3	0.1	0.1	-	-	-
650.4	5	0.40	0.15	0.15	0.2	0.1	0.1	-	-	-
645.3	5	0.50	0.13	0.13	0.1	0.1	0.1	-	-	-
640.3	5	0.42	0.11	0.11	0.1	0.1	0.1	-	-	-
635.2	5	0.48	0.18	0.18	0.1	0.1	0.1	-	-	-
625.0	5	0.53	0.22	0.22	0.2	0.1	0.1	-	-	-
614.9	5	0.38	0.28	0.28	0.1	0.0	0.0	-	-	-
1394.2	6	0.80	0.07	0.07	5.2	0.5	0.5	-	-	-
1388.6	6	0.88	0.05	0.06	5.2	0.4	0.4	-	-	-
1384.4	6	0.78	0.05	0.05	5.3	0.5	0.5	-	-	-
1380.2	6	0.61	0.04	0.05	4.6	0.4	0.4	-	-	-
1377.4	6	0.58	0.05	0.05	5.2	0.5	0.5	-	-	-
1376.0	6	0.49	0.04	0.05	4.9	0.5	0.5	-	-	-
1374.6	6	0.48	0.04	0.04	5.3	0.5	0.5	-	-	-
1373.2	6	0.49	0.05	0.05	5.3	0.5	0.5	-	-	-
1371.8	6	0.53	0.04	0.04	5.0	0.4	0.4	-	-	-
1369.0	6	0.80	0.06	0.06	5.0	0.5	0.5	-	-	-
1364.9	6	0.90	0.05	0.06	5.1	0.5	0.5	-	-	-
1360.7	6	0.95	0.06	0.06	4.6	0.5	0.5	-	-	-
1355.1	6	1.07	0.10	0.10	5.3	0.5	0.5	-	-	-
884.3	6	1.23	0.06	0.07	1.6	0.3	0.3	-	-	-
880.9	6	1.27	0.06	0.07	1.5	0.2	0.2	-	-	-
878.6	6	1.17	0.06	0.07	1.6	0.3	0.3	-	-	-
876.3	6	1.08	0.06	0.07	1.1	0.2	0.2	-	-	-
875.2	6	0.98	0.05	0.06	1.4	0.3	0.3	-	-	-
874.1	6	0.89	0.05	0.06	1.3	0.2	0.2	-	-	-
873.0	6	0.92	0.05	0.06	1.2	0.3	0.3	-	-	-
870.7	6	1.13	0.06	0.07	1.2	0.2	0.2	-	-	-
866.2	6	1.23	0.08	0.08	1.3	0.2	0.2	-	-	-
861.8	6	1.35	0.08	0.08	1.3	0.3	0.3	-	-	-

856.2	6	1.41	0.08	0.08	1.3	0.3	0.3	-	-	-

2023 Determination of the excitation functions for nuclear reactions induced by helium-3 in lithium José Grilo

NOVA
NOVA SCHOOL OF
SCIENCE & TECHNOLOGY